Bull Volcanol (2011) 73:983–1003
DOI 10.1007/s00445-011-0504-x

RESEARCH ARTICLE

Fragmentation in kimberlite: products and intensity of explosive eruption

Stephen Moss · J. K. Russell

Received: 1 February 2010 / Accepted: 14 April 2011 / Published online: 25 September 2011

Abstract The explosive eruption of kimberlite magma is capable of producing a variety of pyroclast sizes, shapes, and textures. However, all pyroclastic deposits of kimberlite comprise two main types of pyroclasts: (1) pyroclasts of kimberlite with or without enclosed olivine crystals and (2) olivine crystals which lack coatings of kimberlite. Here, we propose two hypotheses for how kimberlite magmas are modified due to explosive eruption: (1) olivine crystals break during kimberlite eruption, and (2) kimberlite melt can be efficiently separated from crystals during eruption. These ideas are tested against data collected from field study and image analysis of coherent kimberlite and fragmental kimberlite from kimberlite pipes at Diavik, NT. Olivines are expected to break because of rapid pressure changes during the explosive eruption. Disruption of kimberlite magma, and pyroclast production, is driven by ductile deformation processes, rather than by brittle fragmentation. The extent to which melt separates from olivine crystals to produce kimberlite-free crystals is a direct consequence of the relative proportions of gas, melt and crystals. Lastly, the properties of juvenile pyroclasts in deposits of pyroclastic kimberlite are used to index the relative intensity of kimberlite eruptions. A fragmentation index is proposed for kimberlite eruption based on: (a) crystal size distributions of olivine and on (b) ratios of selvage-free olivine pyroclasts to pyroclasts of kimberlite with or without olivine crystals.

Keywords Kimberlite · Fragmentation · Olivine · Juvenile pyroclast

Editorial responsibility: R.S.J. Sparks

This paper constitutes part of a special issue:

Cas RAF, Russell JK, Sparks RSJ (eds) Advances in kimberlite volcanology and geology.

S. Moss · J. K. Russell
Volcanology and Petrology Laboratory, Department of Earth and Ocean Sciences, The University of British Columbia,
6339 Stores Road,
Vancouver, BC V6T 1Z4, Canada

S. Moss (✉)
Mineral Services Canada Inc.,
205-930 Harbourside Drive,
North Vancouver, BC V7P 3S7, Canada
e-mail: stephen.moss@mineralservices.com

J. K. Russell
Mineral Deposit Research Unit, Department of Earth and Ocean Sciences, The University of British Columbia,
6339 Stores Road,
Vancouver, BC V6T 1Z4, Canada

Introduction

Eruptions of kimberlite volcanoes are poorly understood. There have been no historical eruptions of kimberlite, and kimberlite volcanoes are rarely preserved. As a consequence, the styles of explosive eruption of kimberlite magma are not documented directly. In particular, the mechanisms of fragmentation have not been established for explosive eruption of kimberlite. However, mining of kimberlite pipes for diamonds has allowed detailed petrographic and mineralogic observations of rock textures and pyroclastic products produced by kimberlite eruptions. Here, fragmentation processes in explosive kimberlite eruptions are explored by making observations on pyroclastic kimberlite. Pyroclastic products of kimberlite eruptions from around the world (Table 1) are diverse and characterized by the following. They:

- Comprise a limited size range of pyroclasts relative to pyroclastic deposits of other magma types (Fig. 1a, b)

Table 1 Summary of key observations of kimberlite pyroclasts that constrain the nature of eruptions

Attribute	Where observed/described	Notes	Reference
1. Deposits contain fine ash-size particles	Ekati, Diavik, NT	Rounded, in accretionary lapilli (described)	Moss et al. 2008; Porritt et al. 2008
	Star, SK, Canada	Fine ash-sized olivine (described)	Harvey et al. 2009; Zonneveld et al. 2004
	Orapa, Botswana	Vesicular, amoeboid (described)	Gernon et al. 2009
	Aries, WA, Australia	Inferred ash (interpreted)	Downes et al. 2007
	Tokapal, India	Serpentinized ash (described)	Mainkar et al. 2004
2. Deposits lack large (>50 mm) pyroclasts	Diavik, NT, Canada	Up to 50 mm	Moss et al. 2008
	Venetia, South Africa; Mwadui, Tanzania	Lithics <20 cm, olivine <4 mm; up to 18 mm	Walters et al. 2006; Stiefenhofer and Farrow 2004
	Star/Orion, SK, Canada	Used to recognize individual eruptions	Kjarsgaard et al. 2009
3. Deposits contain abundant 'free' or liberated olivine crystals	Ekati, Diavik, NT, Canada	Dominant	Porritt et al. 2008; Nowicki et al. 2004; Moss et al. 2008, 2009
	Orapa, Botswana; Mothae, Lesotho	Present; low to moderate abundance in sedimentary rocks	Brown et al. 2008; Galloway et al. 2009
	Star, SK, Canada		Zonneveld et al. 2004
4. Olivine crystal shapes range from rounded to angular	Victor, ON, Canada	Broken crystals in apparent coherent rocks	van Straaten et al. 2008
	Diavik, Ekati, NT, Canada	Minor shape modif.; angular in VK rocks	Moss et al. 2008; Nowicki et al. 2008
	Venetia, South Africa	Rounded or highly fractured	Walters et al. 2006
	Orapa, Botswana	Rounded to broken	Brown et al. 2008
	Udachnaya, Russia	Broken crystals	Kamenetsky et al. 2008
5. Deposits have variable ratios of 'free' olivine crystals to clots of crystallized kimberlite melt	Diavik, Ekati, NT; Victor, ON, Canada	Measured	Moss et al. 2009; Nowicki et al. 2008; Webb et al. 2004
	Kimberley, South Africa; Mwadui, Tanzania	Described	Clement 1982; Stiefenhofer and Farrow 2004
	Buffalo Head Hills, AB, Canada	Described	Boyer et al. 2004
	Star, Orion, SK, Canada	Var. b/w volcaniclastic deposits; described	Zonneveld et al. 2004; Pittari et al. 2008
6. Juvenile pyroclasts (JP) contain variable amounts of vesicles	Diavik, NT, Canada; Mothae, Lesotho	Variably vesicular	Moss et al. 2008, 2009; Galloway et al. 2009
	Attawapiskat, Victor, ON, Canada	Present, minor	van Straaten et al. 2008
	Aries, WA, Australia; Tokapal, India	Present	Downes et al. 2007; Mainkar et al. 2004
	FALC, Sturgeon Lake, SK, Canada	Present to abundant	Leckie et al. 1997; Scott Smith 2008a, b; Scott Smith 1995
	Buffalo Head Hills, AB, Canada	Present	Boyer et al. 2004; Field and Scott Smith 1999
7. JPs have spherical external morphologies	Victor, ON, Canada	Photographs	Webb 2006
	Diavik, Ekati, NT, Canada	Dominant; rounded but also elongate	Moss et al. 2008; Nowicki et al. 2008
	Mountain Lake, AB, Canada	Typically cored by single olivine crystal	Wood et al. 1998
8. JPs have 'amoeboid' or irregular external morphologies	FALC, Candle Lk, Sturgeon Lk, SK, Canada	Abundant; present; curvilinear to amoeboid	Field and Scott Smith 1999; Mitchell 2009
	Buffalo Head Hills, AB, Canada	Present	Boyer et al. 2004; Field and Scott Smith 1999
	Ekati, NT, Canada	Maybe due to alteration	Porritt et al. 2008

Table 1 (continued)

Attribute	Where observed/described	Notes	Reference
9. Olivine crystals have complete or partial selvages of melt	Gahcho Kue, Diavik, Ekati, NT, Canada	Abundant in 'TK'; ubiquitous; 'cored' clasts	Hetman et al. 2004; Moss et al. 2009; Nowicki et al. 2008
	Pimenta Bueno, Brazil; Renard, OC, Canada	Abundant in 'TK'	Masun and Scott Smith 2008; Fitzgerald et al. 2009
	Koffiefontein, Letlhakane, South Africa	'Pelletal' lapilli with very thin rims in crystal-supported rocks; photographs	Naidoo et al. 2004; Trickett et al. 2006
	Yakutia, Russia		Kurszlaukis et al. 2006
10. Deposits contain accretionary lapilli	Diavik, Ekati, DO-27, NT, Canada	Present to rare	Moss et al. 2008; Porritt et al. 2008; Harder et al. 2009
	Jwaneng, Botswana; Archangelsk, Russia	Rare	Webb et al. 2004; Mahotkin et al. 2003
	Buffalo Head Hills, AB, Canada	Present	Boyer et al. 2004
	Venetia, South Africa	Abundant	Kurszlaukis and Barnett 2003

- Can contain fine ash, although it is commonly a poorly preserved component of deposits (Fig. 1a)
- Contain pyroclasts with morphologies that are dominantly spherical to sub-spherical, or even amoeboid shaped (Fig. 2a, b, c, d)
- Comprise juvenile pyroclasts of kimberlite that have highly variable ratios of olivine crystal/kimberlite groundmass (Fig. 1g, h)
- Contain pyroclasts with variable (0 to 20%) amounts of internal vesiculation (Fig. 1e, f)
- Can be dominated by 'kimberlite-free' olivine crystals (Fig. 2g, h)
- Can contain, albeit rarely, accretionary lapilli (Fig. 1c, d) comprising sub-millimetre-sized angular olivine fragments and fine ash-sized particles
- Can contain pyroclasts of olivine crystals that are partially to fully coated by a selvage of kimberlite (Fig. 2e, f)

From such observations, it is clear that kimberlite eruptions are capable of producing a variety of pyroclast types. Any hypothesis regarding the manner(s) in which kimberlite magma is disrupted must address this textural diversity. Olivine crystals and crystal fragments are volumetrically important in kimberlite magma and are a dominant trait of pyroclasts; kimberlite pyroclasts range from kimberlite-free crystals of olivine to olivine-free clots of solidified kimberlite magma. Discussions of kimberlite eruption styles must thus consider properties of these two pyroclast types.

Here, two hypotheses are proposed for how kimberlite magmas are modified due to explosive eruption: (1) olivine crystals break during kimberlite eruption and (2) kimberlite melt can be efficiently stripped from crystals during eruption. These ideas are tested against data collected from field study and image analysis of coherent kimberlite interpreted as dykes (CK; Moss et al. 2010) and fragmental kimberlite interpreted as a primary pyroclastic deposit (PK; Moss et al. 2009) within a kimberlite pipe at Diavik, NT. Based on these data, possible controls on the formation and modification of pyroclasts during eruption are discussed. Olivines are expected to break at intrinsic places of weakness because of rapid pressure changes during explosive eruption. Disruption of kimberlite magma into pyroclasts is driven by ductile deformation processes, rather than by brittle fragmentation. The extent to which the olivine crystal cargo is stripped of melt depends on the relative proportions of gas, melt and crystals. Finally, properties and proportions of juvenile pyroclasts in deposits of pyroclastic kimberlite are used to index the relative intensity of kimberlite eruptions. Specifically, a fragmentation index is proposed for kimberlite eruptions based on: (a) olivine crystal populations and (b) ratios of 'free' olivine crystals to pyroclasts of solidified kimberlite magma (with or without olivine crystals).

Olivine fragmentation during explosive eruption

Angular crystals are common components of pyroclastic rocks (Cas and Wright 1987; Best and Christiansen 1997; Schmincke 2004). Crystal breakage during explosive volcanic eruption has been attributed to crystal-to-crystal

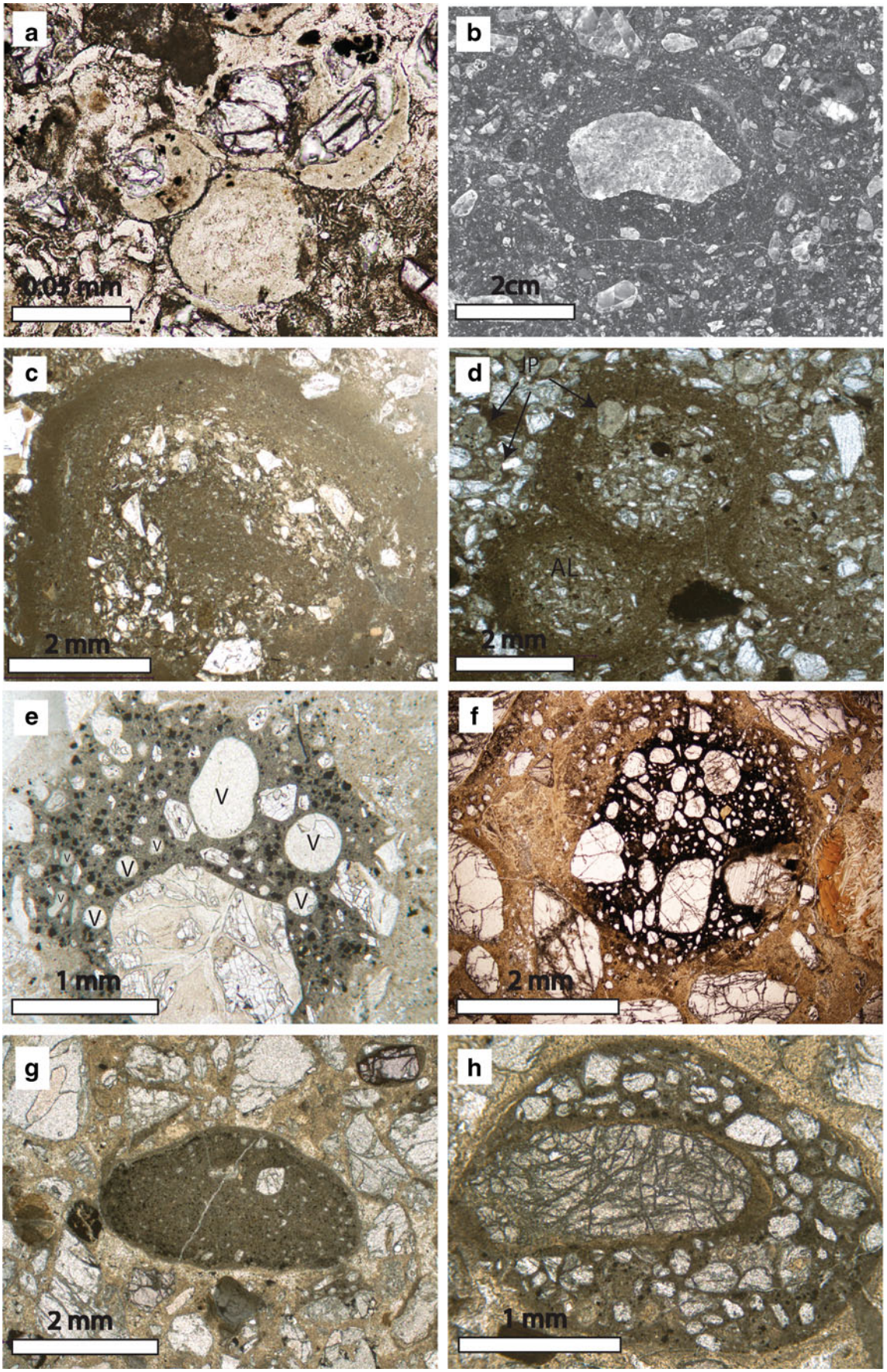
a
0.05 mm
b
2cm
c
2 mm
d
P
AL
2 mm
e
V
V
V
V
V
V
V
1 mm
f
2 mm
g
2 mm
h
1 mm

◀ **Fig. 1** Photomicrographs showing types of juvenile pyroclasts derived from explosive eruption of kimberlite magma in A154N, Diavik, NT: **a** very fine ash-sized (<0.1 mm in diameter), round juvenile pyroclasts of kimberlite cored by olivine crystals; **b** large juvenile pyroclast (>3.5 cm in diameter) cored by peridotite xenolith; **c** large, concentrically zoned, rim-type accretionary lapillus (sensu Schumacher and Schmincke 1991) comprising a core of very fine-grained ash, a central band of olivine crystal fragments, and outer rims of successively finer-grained ash particles; **d** multiple rim-type accretionary lapilli (*AL*) comprising olivine crystal fragments, fine ash-sized juvenile pyroclasts of kimberlite (*JP*), and very fine-grained ash; **e** vesiculated juvenile pyroclast (*v*) featuring serpentinized olivine crystals and groundmass spinel crystals; **f** dense, non-vesiculated and olivine crystal-rich juvenile pyroclast with a serpentinized outer edge; **g** crystal-poor pyroclast of kimberlite; **h** crystal-rich juvenile pyroclast of kimberlite cored by garnet xenocryst

interactions in volcanic vents, plumes and flows and the expansion of melt and mineral inclusions due to rapid decompression (Best and Christiansen 1997; Bindeman 2005). Angular and internally fractured olivine crystals are common in kimberlite deposits (Webb et al. 2004; Nowicki et al. 2008) and are interpreted to result from explosive magmatic eruption (e.g. Pittari et al. 2008), phreato-magmatic explosions (e.g. van Straaten et al. 2008), decompression associated with intrusive emplacement (e.g. Basson and Viola 2004), and secondary reworking of primary deposits (e.g. Boyer et al. 2004).

Preliminary observations of coherent and fragmental rocks in the A154N kimberlite volcano at Diavik, NT, suggest olivine crystal shapes and sizes in coherent rocks are different than those observed in some fragmental rocks (Fig. 3). For example, olivine crystals in dykes of CK are ellipsoidal in shape, vary from round to sub-round, cover a large size range, and have a characteristic crystal size distribution (CSD) slope (Moss et al. 2010). In contrast, olivine crystals from pyroclastic kimberlite (PK) in A154N range from sub-round to angular, may comprise smaller sizes, and are, internally, highly cracked or fractured (Moss et al. 2010). The PK and CK reside in the same volcano and are approximately the same age (Graham et al. 1999). Assuming that the olivine crystal contents in the magmas that produced the pyroclastic rocks are the same as those forming intrusive dykes of coherent kimberlite within A154N, then the crystal populations from PK and CK can be used to evaluate the effects of volcanic eruption on olivine crystal shapes, sizes, and overall population properties.

Methods

The working hypothesis is that olivine crystals break during eruption of kimberlite magma. To test this hypothesis, field study and image analysis are used to characterize olivine crystal populations in CK intrusions and pyroclastic rocks (PK) from the A154N kimberlite at Diavik. For olivine in coherent rocks, data collected by Moss et al. (2010) are used. Data on olivine in pyroclastic rocks are from Moss et al. (2008, 2009). Using image analysis techniques described in Moss et al. (2010), the olivine grains within each sample are measured for size (area, A), perimeter (P), crystal shape as defined by circularity $(4\pi \cdot A)/P^2)$, combined modal area per cent (%), and cumulative grain size distributions (i.e. frequency, area).

Comparison of the CK and PK datasets is on the basis of crystal size distribution plots, descriptive numerical parameters, and statistical descriptors of shape (Tables 2 and 3). This allows us to test if eruption changes the sizes, shapes, and overall population characteristics of olivine CSDs.

Results

To characterize overall differences in the two populations, conventional grain size parameters from sedimentology and volcanology are used (Table 2; Inman 1952). The comparative properties of the olivine populations are shown in Fig. 4 and summarized in Table 2.

A plot of cumulative frequency vs. size shows an overall finer size distribution for olivines in PK than in CK (Fig. 4a); crystals ≥1 mm^2 comprise 68% of CK olivines but only 27% of PK olivines by area. PK olivine crystals have a smaller median size (MdΦ=4.0 vs. 3.8), are more poorly sorted (σ=3.6 vs. 3.5), and are more skewed in distribution (α=0.8 vs. 0.5) than olivine crystals from CK (Table 2). Log–log plots of cumulative frequency vs. size show olivine in coherent kimberlite to approximate power–law distributions[1] (Fig. 4b), with a characteristic slope (D) and intercept (λ) relationship (Moss et al. 2010). Power–law equations are fitted to olivine crystals in PK, and the values of slope (D) and intercepts (λ) are shown in Fig. 4c and Table 2. A comparison of power–law slopes (D) and intercepts (λ) shows an increase in slope (3.61 to 4.29) and a decrease in the intercept (−2.38 to −2.60) for olivine crystals from CK to PK (Table 2).

Crystal shapes for olivine from CK and PK are compared in Fig. 4d and Table 2 in terms of circularity (0–1, where a perfect circle is 1). PK olivine circularity ranges from 0.25 to 0.99, with a geometric mean (μ) of 0.73, and are well described by a normal, Gaussian distribution. CK olivines show circularity ranges from 0.2 to 0.99, with a geometric mean value (μ) of 0.61, and are inconsistent with a normal distribution. Comparison of the standard deviation of data about the mean circularity

[1] There are many two-parameter model equations which appear similar over small ranges of observation (e.g. gamma, power, log-normal) (Bonnet et al. 2001; Clauset et al. 2007). Here, power–law equations of the form $N_v(X \geq x) = \lambda x^{-D}$ are used to approximate, rather than describe, olivine crystal populations after Moss et al. (2010).

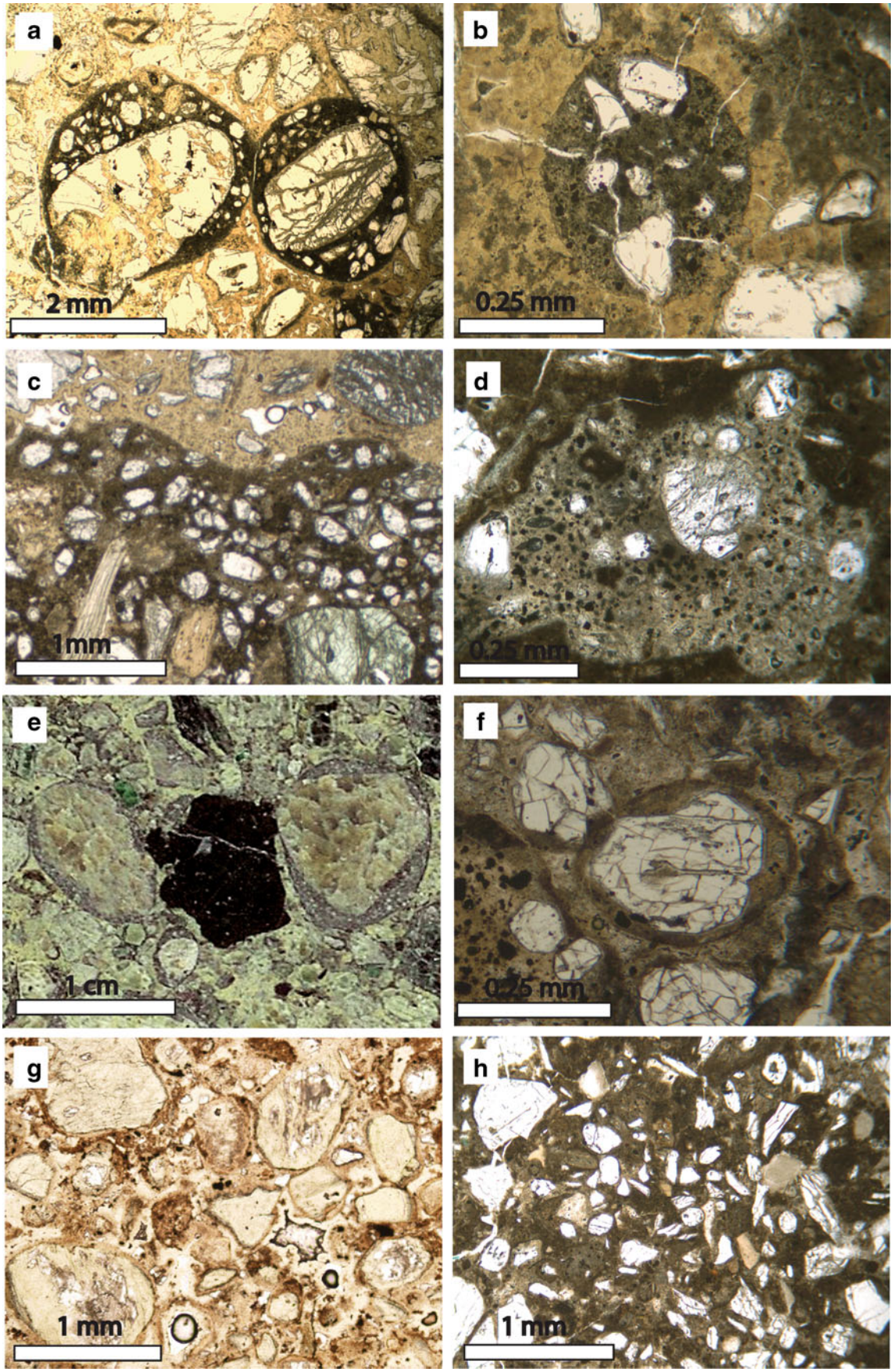
a
2 mm
b
0.25 mm
c
1mm
d
0.25 mm
e
1 cm
f
0.25 mm
g
1 mm
h
1 mm

◀ **Fig. 2** Photomicrographs showing morphologies of juvenile pyroclasts derived from explosive eruption of kimberlite magma in A154N, Diavik, NT: **a** round juvenile pyroclasts of kimberlite cored by olivine crystals; **b** round, fine ash-sized juvenile kimberlitic pyroclast enclosing multiple small (<0.125 mm in diameter) olivine crystals, in a matrix of serpentine; **c** curviplanar margin of juvenile pyroclast; **d** 'amoeboid'-shaped, ash-sized juvenile kimberlitic pyroclast containing vesicles, olivine crystals, and groundmass spinel; **e** pyroclasts comprising partial and complete selvages of kimberlite coating centimetre-scale olivine crystals; **f** fine ash-sized juvenile pyroclast with complete, thin (<0.125 mm) selvage of kimberlite coating olivine; **g** round, serpentinized olivine crystals in a crystal and clast-supported matrix; **h** sub-round to angular, fresh olivine crystals and ash-sized juvenile pyroclasts of kimberlite in a fine-grained matrix

suggests that the two populations are distinct and that olivines in PK are more rounded than olivines in CK. Comparison of 3D axial ratios for the two olivine populations is accomplished using CSDSlice™ (Morgan and Jerram 2006). In the CSDSlice™ database, a minimum of 10,000 slices are taken through poly-disperse (sensu Higgins 2000), randomly oriented model populations created from over 700 crystal shapes; these data are compiled in a database and used to identify the 3D axial ratio which best represents 2D olivine crystal intersection data from CK and PK. CSDSlice™ shows 2D intersection data from CK olivines to be best approximated by a 1:1:1 ratio, which is statistically indistinguishable from PK olivines (1:1:1; Table 2).

Table 2 Properties of olivine within CK and PK_2

Property	CK	PK_2
Area (%)	46.7–51.2	39.4
Size range (mm)	0.03–12.4	0.025–15.16
ol(n)/OL(n[a])	72:1 to 138:1	248:1
MdΦ[b]	3.3–3.8	4.0
σ[c]	2.9–3.5	3.6
α[d]	0.3–0.5	0.8
D[e]	3.53–3.61	4.29
λ[f]	2.22–2.38	2.60
RMSE[g]	0.16–0.31	0.28
3D shape (R^2)	1:1:1 (~0.8)	1:1:1 (0.83)

3D aspect ratios and correlation coefficients obtained using CSDSlice (Morgan and Jerram 2006)

[a] ol=olivine <1 mm, DL=olivine ≥1 mm

[b] MdΦ=median phi size ($-\log_2(d)$)

[c] σ=sorting efficiency=$\frac{(\phi_{84})-(\phi_{16})}{2}$

[d] α=skewness=$\frac{(\phi_{84})+(\phi_{16})-Md\phi}{\sigma}$

[e] D=slope of best-fit power–law

[f] λ=intercept of best-fit power–law

[g] Root mean standard error

Melt-stripping of olivine during explosive eruption

A large proportion of the juvenile pyroclasts found in deposits of kimberlite occur as individual crystals of olivine having no kimberlite selvages. Here, we use 'free' crystals to denote such crystals that were derived directly from the kimberlite magma but were liberated or separated from the melt because of eruption. Such crystals are common in many highly energetic volcanic eruptions (Cas and Wright 1987). However, the free crystal pyroclasts found in kimberlite are unique relative to free crystals of plagioclase, quartz, and hornblende found in most andesite and dacite systems (e.g. Fisher 1963; Heiken 1972; Blake et al. 1992; Hammer et al. 2006; Dunbar et al. 2008; Michol et al. 2008) because: (a) they feature little to no coating or selvage of glass or crystallized melt and (b) if a selvage is present, it is spheroidal to curviplanar in external morphology and commonly vesicle free (Figs. 1 and 2).

In addition to free crystals, other juvenile pyroclasts derived from kimberlite eruptions show a variety of textural relationships between olivine crystals and quenched or

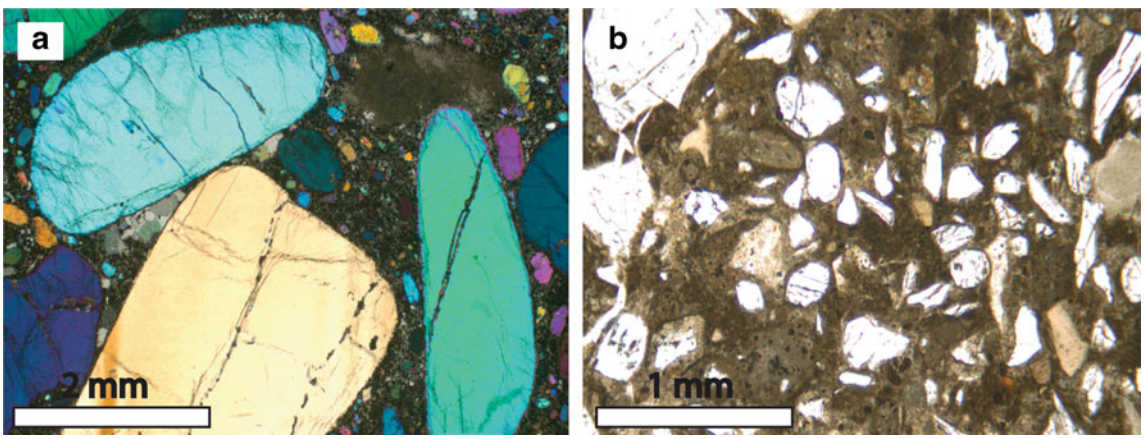

Fig. 3 Photomicrographs illustrating differences in shapes of olivine grains within: **a** coherent and **b** pyroclastic kimberlite from Diavik kimberlite pipes

Table 3 Representative olivine content in: CK, PK_2, and JP of crystallized kimberlite

Sample	Area%			Area%		
	ol	gm	ol/gm	'free' ol	jp	ol/jp
CK01[a]	50.0	43.7	1.1			
CK02[a]	48.2	44.1	1.1			
CK03[a]	48.1	40.3	1.2			
CK04	46.7	42.4	1.1			
CK05	51.2	38.8	1.3			
CK_AVG	48.9	41.9	1.2			
PK_330[b]				26.9	3.9	6.9
PK_340[b]				53.2	2.3	22.9
PK_350[b]				56.9	1.3	43.8
PK_360[b]				26.1	5.1	5.1
PK_370[b]				32.9	5.2	6.3
PK_380[b]				35.2	18.2	1.9
PK_TOT[c]				35.8	5.4	6.7
JP_TOT[d]	66.3	33.7	2.0			
PKJP_TOT[e]	39.4	1.8	22.4			

Olivine content measured as area per cent from slab and t.s.

[a] Replicate samples from a single dyke; gm=groundmass

[b] Representative sample horizons within 50-m-thick PK_2

[c] Linear combination of ten samples at 5-m intervals in PK_2

[d] Linear combination of olivine in JPs from PK_2

[e] Combined modal per cent of olivine in PK and resident JP in PK_2

crystallized kimberlite (Figs. 1 and 2). For example, olivine crystals can form the cores of juvenile pyroclasts of kimberlite or can be partially or completely enclosed by a thin jacket or selvage of kimberlite (Webb 2006; Moss et al. 2008). Olivine-free juvenile pyroclasts of kimberlite are rare and typically ash or fine ash in size (Moss et al. 2009). To simplify the array of sizes, shapes, and crystal and selvage textures observed in kimberlite deposits, we refer hereafter to pyroclasts comprising olivine crystals with any coating of kimberlite as 'juvenile pyroclasts' or JPs. Though 'free' olivine crystals are technically also juvenile pyroclasts, we hereafter refer to them as free olivines or FO.

The sizes, abundances, and morphologies of JPs can vary significantly, even within a single pyroclastic deposit (Moss et al. 2008; Mitchell 2009; Porritt and Cas 2009). Moreover, the amount of FO relative to ash and lapilli-sized JPs can also vary from deposit to deposit (Webb et al. 2004; Scott Smith 2008a; Scott Smith and Smith 2009). In some cases, deposits may comprise almost exclusively FO, while other deposits comprise abundant JPs (e.g. Fig. 5). In addition, alteration and textural modification can mask true textural relationships. The occurrence of FO and JP together in virtually all pyroclastic deposits of kimberlite (e.g. Table 1), however, suggests olivine crystals are liberated from melt during all explosive kimberlite eruptions. Based on these global observations, it is hypothesized that melt is separated from olivine crystals during explosive kimberlite eruption.

Methods

To test this hypothesis, data collected from a primary pyroclastic deposit (PK) from the A154N kimberlite pipe (Moss et al. 2008, 2009) are compared with olivine abundance data from CK. A low degree of alteration and textural modification within the CK and PK of A154N allow for a detailed textural study of this kind. The PK data include modal abundances of FO and JPs, and these data are used to investigate the ratio of FO to JPs within the entire PK deposit (Table 3). We also want to estimate the volumetric ratio of all olivine crystals (free and within pyroclasts) to the kimberlite coating attached to olivine (e.g. within JP; Table 3). To evaluate this ratio, we use image analysis methods from Moss et al. (2009). These methods are used to characterize over 200 kimberlitic pyroclasts from ten different thin sections sampled at 5-m vertical intervals throughout the PK. The measurements include the size and modal abundance (area per cent) of the individual olivine grains, as well as the total surface areas (SA_{ol}) of the olivine content *within* each juvenile pyroclast. Assuming that juvenile pyroclasts observed in thin sections are representative of the entire PK deposit allows us to determine the total area per cent of kimberlite coating attached to olivine. The measurements of olivine modal per cent and SA_{ol} within each juvenile pyroclast also allow for evaluation of whether olivine abundance influences the ability of melt to separate from crystals. These data are then compared with olivine to groundmass ratios in CK to establish how much melt was separated from the olivine crystals during the PK-producing eruption.

Results

Results are shown in Table 3. Ratios of FO to JPs in PK range from ~2:1 to >40:1. Combining all samples in PK shows an FO/JP ratio of 6.7. Figure 6 is a plot of juvenile pyroclast size (area in square millimetres) vs. its enclosed olivine content for two pyroclastic deposits from A154N (i.e. PK and PK1; Moss et al. 2009). Overall, there is no correlation between 2D size and enclosed olivine content; pyroclasts can have any 2D size to olivine content relationship, except for some extreme ratios (Fig. 6a). The combined modal percentage of olivine crystals in juvenile pyroclasts yields a 2:1 ratio of olivine crystals to groundmass in juvenile pyroclasts (Table 3). Assuming that the area per cent ratio of olivine content to kimberlite measured within the juvenile pyroclasts in this study is representative

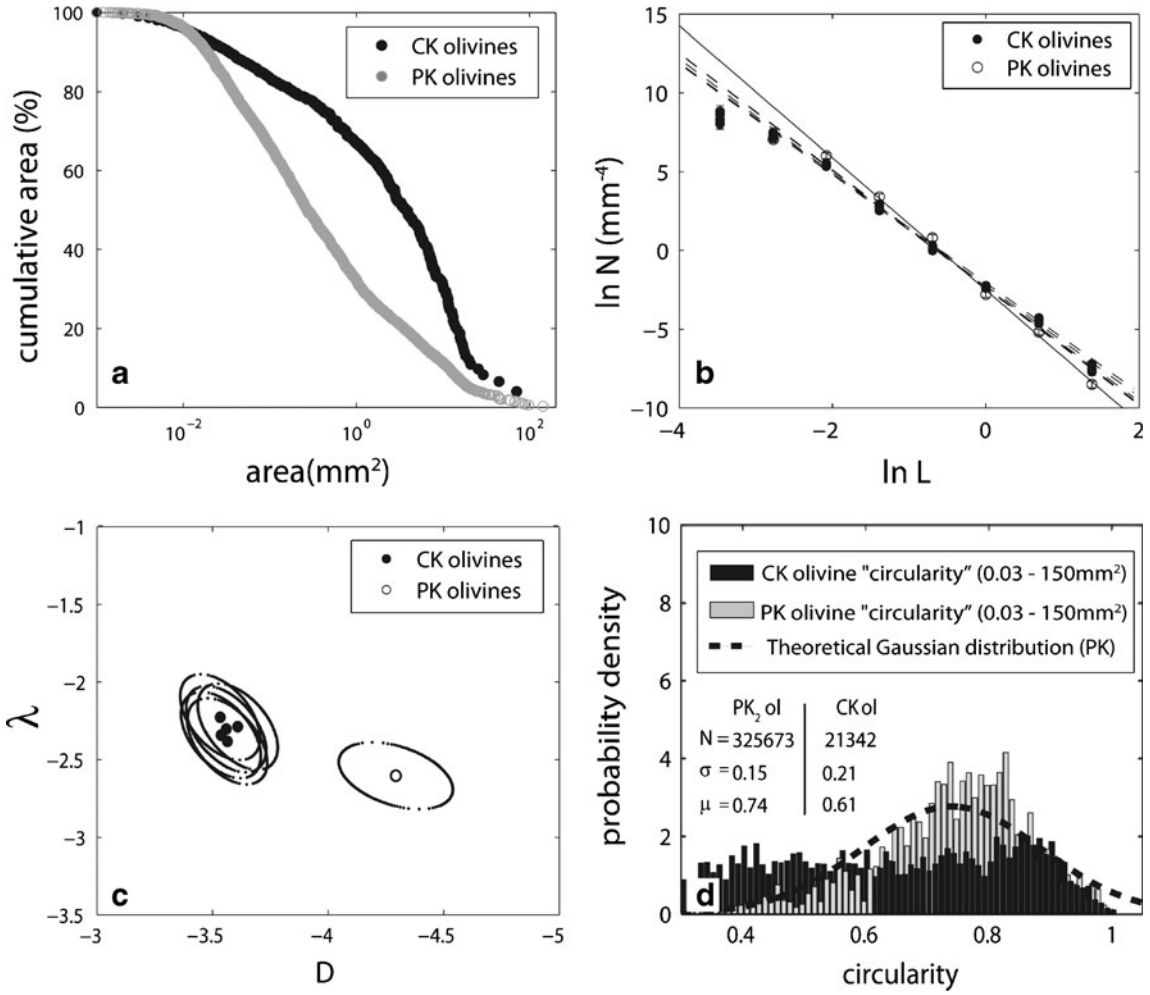

Fig. 4 Tests for modification of olivine crystal populations observed in coherent kimberlite (*CK*) due to explosive volcanic eruption and represented by olivines in pyroclastic kimberlite (*PK*): **a** cumulative area per cent vs. area (square millimetres); **b** ln N (mm^{-4}) vs. ln L data fitted to power–law distributions (*CK*, *dashed lines*; *PK*, *solid line*; see text). Analytical errors are smaller than symbol size; **c** parameters to power–law models in **b** (λ, intercept; *D*, slope) showing calculated covariance envelopes (after Moss et al. 2010); **d** histograms of circularity for individual olivine crystals based on truncated size distributions (0.03–150 mm^2) for *CK* (*black*) and *PK* (*grey*) deposits. The PK dataset is fitted to a normal Gaussian distribution (*heavy dashed line*). The *inset table* shows number of crystals (*N*), standard deviation (σ), and mean circularity (μ) of olivine grains in PK and CK

and can be applied to all juvenile pyroclasts from PK, the total (FO + olivine inside JPs) olivine to kimberlite ratio for PK is >22:1 (Table 3). In contrast, ratios of olivine crystals to kimberlite groundmass in CK are ~1:1 relationships (Table 3). The implication is that, if olivine to groundmass ratios in the PK-producing magma were similar to the ratios measured in CK rocks (Table 3), over 90% of the melt fraction may have been separated from olivine crystals during eruption.

Discussion

In this section, we discuss implications of the observations described above. First, factors which may encourage breaking of olivine crystals are discussed. Secondly, ideas are developed to show how the properties of kimberlite magma during eruption can explain the observed shapes, sizes, textures, and abundances of juvenile kimberlite pyroclasts.

Olivine fragmentation

Olivine crystals measured in pyroclastic kimberlite rocks show clear differences from those measured in intrusive coherent kimberlite. Shape indices, population parameters, and crystal size distribution model equations all indicate a fundamental difference in the olivine crystal populations from CK and PK. The simplest explanation is that the explosive eruption of kimberlite magma modifies the

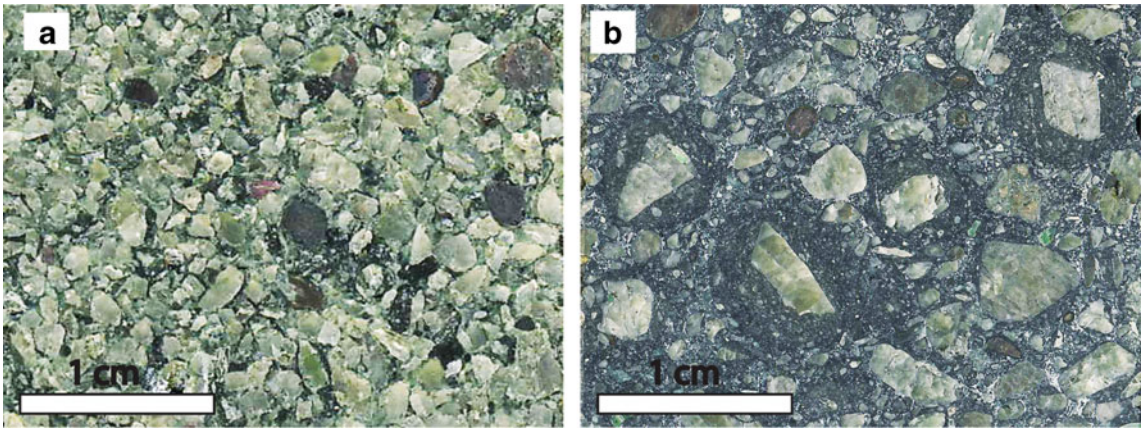

Fig. 5 Variable crystal–kimberlite relationships in pyroclastic kimberlite deposits from Diavik, NT: **a** abundant 'free' olivine crystals in a poorly sorted, crystal-supported matrix; **b** abundant olivine-cored juvenile pyroclasts of kimberlite within a poorly sorted, crystal and clast-supported matrix

shapes, sizes, and overall population characteristics of olivine crystals. Here, we discuss the properties of olivine crystals in kimberlite magma which can cause crystals to break. Then, we discuss potential controlling factors responsible for differences in the populations of olivine crystals observed in pyroclastic deposits.

Properties of olivine crystals in kimberlite magma

Olivine crystals in kimberlite have several physical attributes which lend themselves to shape and size modification during explosive eruption. First, the majority of olivine crystals in kimberlite magma are xenocrystic and derived from the lithospheric mantle (Arndt et al. 2006; Kamenetsky et al. 2007; Brett et al. 2009). As such, many crystals store stresses imposed by mantle processes as evidenced by undulose extinction or appear to have accommodated stress by cracking or fracturing, though incompletely (Fig. 7a, b). Detailed petrography of olivine crystals in coherent and fragmental rocks at Diavik has indicated evidence of crack-healing and crack-sealing within olivine crystals. Second, olivine crystals in kimberlite magma also contain abundant mineral and melt inclusions (Fig. 7c). Together, these physical characteristics act as points, lines, and planes of intrinsic weakness within individual olivine crystals (e.g. Fig. 7d).

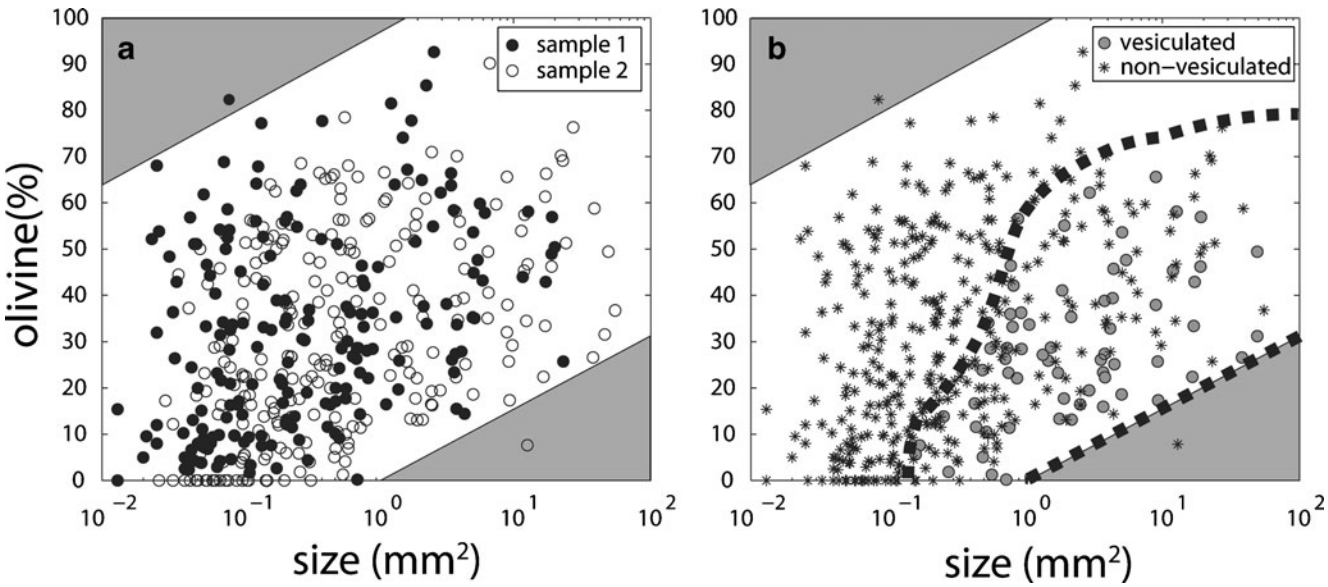

Fig. 6 Parametric analysis of JPs from PK (sample 1) and PK_1 (sample 2) of A154N: **a** olivine (%) vs. size (mm^2). *Shading* denotes regions of no data. **b** Olivine content (%) vs. size (mm^2) of juvenile pyroclasts from both samples classified as vesiculated and non-vesiculated. The field defined by *dashed lines* encloses all vesiculated (v) pyroclasts

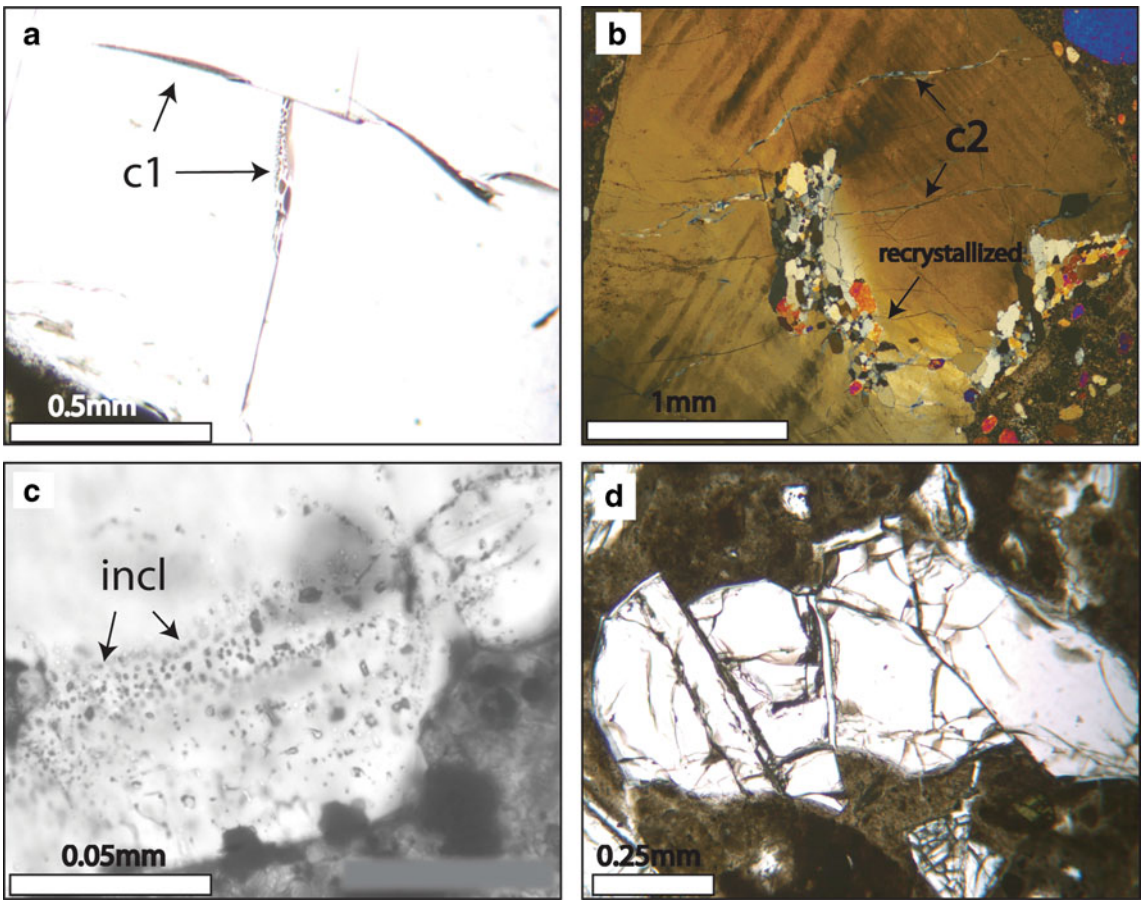

Fig. 7 Properties of olivine crystals contributing to crystal breaking during eruption: **a** partially healed (*c1*) cracks within olivine from CK terminate before edge of crystal; **b** cross-polarized photomicrograph of large, strained olivine macrocryst within CK containing cracks filled with carbonate (*c2*) and internal zones of recrystallized olivine; **c** melt and mineral inclusions (*incl*) in an olivine overgrowth; **d** angular, fractured olivine within PK of A154N

Explosive volcanic eruption and olivine populations

Experiments have shown the slopes of particle size distributions in log–log plots (i.e. *D* values) to correlate positively with the magnitude of pressure drop attending fragmentation (Kueppers et al. 2006) and the number of fragmentation generations (Kaminski and Jaupart 1998). Furthermore, models that simulate the effects of fragmentation on known olivine CSDs suggest a positive increase in the CSD slope due to fragmentation (Moss et al. 2010).

Differences in olivine properties (e.g. *D* values, Inman parameters, crystal shapes) among pyroclastic deposits may result from differences in: (a) the amount of strain, cracks, and inclusions in the pre-eruptive crystals; (b) the pre-eruptive olivine crystal size distributions; or (c) magnitude of pressure drop during emplacement. However, the intrinsic weaknesses in olivine xenocrysts (i.e. stored strain, cracks, inclusions) are also present in olivines within coherent kimberlite (Kamenetsky et al. 2007; Brett et al. 2009). Moreover, olivine crystal size distributions worldwide in coherent kimberlite are believed to be relatively consistent (Scott Smith 2008b, a). Thus, the most likely cause for significant differences in olivine crystal size distributions and shapes in pyroclastic deposits are relative differences in pressure changes.

Crystal–melt separation during eruption

The physical properties of kimberlite magma govern the nature and time scales of magma transport as well as the style of volcanic eruption. Kimberlite is presumed to be a low-viscosity (0.1–10 Pa s), volatile-rich melt (Price et al. 2000; Sparks et al. 2006). Kimberlite magmas can also comprise up to 51% olivine crystals (Moss et al. 2010). Ultimately, kimberlite magmas become 3-phase systems during ascent (gas, liquid melt, crystals); the low-viscosity, high-crystal contents and increasing gas volume fraction can lead to full decoupling of the gas phase from the melt (Vergniolle and Jaupart 1986; Moss et al. 2009). The relative ratios of phases may influence the degree to which melt can separate from olivine crystals, and, thus, most

crystal/groundmass textures observed in pyroclasts derived from kimberlite eruption.

Below, we explore the aspects of each phase (melt, gas, crystals) that can influence primary pyroclast formation and the degree to which melt separates, or 'strips', from crystals, including: (1) melt viscosity, (2) the role of the expanding gas phase in decoupling the melt from olivine crystals, and (3) the role of crystal content (i.e. olivine) in determining the size, shape, and crystal–kimberlite ratios of juvenile pyroclasts.

Viscosity and pyroclast formation

The low-viscosity and high volatile contents of kimberlite melts have important consequences for the formation of pyroclasts. Model viscosities have been calculated (Giordano et al. 2008) for a range of putative kimberlite melt compositions (Price et al. 2000; Russell et al. 2006; Sparks et al. 2006). The calculations were made for kimberlite melts at 1,200°C on an anhydrous basis, as well as using their nominal water contents. Over this wide range of melt compositions, viscosity values were low and varied only slightly (1.5–3 Pa s) regardless of volatile content (Russell et al. 2006).

The temperature dependence of melt viscosity can also be used to estimate the glass transition temperature (T_g) of the melt which is taken as the temperature at which the melt attains a viscosity of 10^{12} Pa s (Giordano et al. 2008). If a melt is cooled to its T_g rapidly enough, crystallization is bypassed, and glass (quenched melt) is produced. The computed range of glass transition temperatures for these same melts is 720–760°C and 690–755°C for anhydrous and volatile-rich equivalents, respectively (Porritt and Russell 2011; Russell et al. 2006). There is very little depression of T_g with increasing H_2O contents. This reflects the fragile nature of these melts and contrasts with the behaviour of basaltic melts where ~2 wt.% H_2O causes a 200°C depression of T_g (Giordano et al. 2008). Normally, the depression of T_g with increased H_2O content provides a simple vehicle for rapid quenching and production of glass during an eruption. Ascent and eruption cause volatile loss and a concomitant increase in T_g to the point that T_g rises to meet magma temperature. At this point, melt is quenched to glass: kimberlite melts do not show the same depression in T_g and thus lack this means of aiding glass formation. In addition, the ΔT between T_{magma} and T_g is higher than in many other magmas (Russell et al. 2006). As a consequence, kimberlite melts can remain molten and fluid longer after disruption or fragmentation than most silicate melts. For this reason, crystal/groundmass relationships and external morphologies (i.e. spherical geometry, contact angle between kimberlite groundmass and crystal) of juvenile pyroclasts are most likely determined by viscous properties such as the surface energy between liquid melt and gas (γ_{m-g}) and the interfacial energy between liquid melt and crystals (γ_{m-x}), rather than brittle failure.

Gas content and melt disruption

Gas content can facilitate separation of kimberlite melt from olivine crystals and disruption of kimberlite melt in several ways (Fig. 8). First, preferred nucleation of the exsolved gas phase on the surfaces of olivine (Blander and Katz 1975) coupled with the high rate of exsolution driven by depressurization of the volatile-rich kimberlite will promote coalescence of adjacent bubbles on a crystal surface. As gas expands and coalesces, it may overcome the interfacial tension between melt and crystal and begin to wet the crystal, thereby displacing the melt (Fig. 8b).

Second, high gas fractions within a low-viscosity melt have been shown to lead to out-gassing through permeability networks or 'gas-streaming' through a body of magma (Herd and Pinkerton 1997; Parfitt 2004; Gonnermann and Manga 2007). Two kinds of fluid mechanical instabilities are created at the interface between a streaming gas and liquid: (1) Kelvin–Helmholz (K–H) instabilities[2], which create waveforms at the interface, and (2) Rayleigh–Taylor instabilities[3] which disrupt liquid from wave crests formed by the K–H instability by rolling-over the crest of the waveforms in a fashion similar to whitecaps on a lake (Villermaux 1998, 2007). Gas streaming can disrupt the kimberlite melt by creating such instabilities along the melt/gas interface due to velocity contrasts between less-dense gas and surrounding kimberlite melt (Fig. 8b, c).

Third, high volatile content, rapid ascent of magma, and narrow conduit geometry could lead to very high exit velocities for the gas phase in erupting kimberlite magma (Sparks et al. 2006; Head and Wilson 2008; Moss et al. 2009). All other factors being equal (e.g. size, gas density, drag coefficient; Wilson and Parfitt 2008), the density (2,700–3,400 kg m^{-3}) of kimberlitic pyroclasts (Cas et al. 2008; Gernon et al. 2008; Moss et al. 2008) would lead to significant settling velocities relative to the partly expanded gas-dominated flux of fragmented magma. We use a sequence of equations as outlined by Bursik (1998) to estimate settling velocities for kimberlite pyroclasts within the expanding eruption column. The drag coefficient is

[2] Kelvin–Helmholz shear instabilities form asymmetric waves at the boundary between gas and liquid of wavelength; $\lambda = \delta\sqrt{\rho/\rho_g}$, where λ is the wavelength, δ is the boundary layer thickness, ρ is the density of the liquid, and ρ_g is gas density.

[3] Rayleigh–Taylor instabilities form as a transverse destabilization of existing waveforms, due to accelerations imposed on the liquid–gas interface by the passage of primary undulations. Such transverse waveforms have a wavelength: $\lambda_\perp/\delta \cong 3We_\delta^{-1/3}(\rho/\rho_g)^{1/3}$, with $We_\delta = \rho_g(\Delta v)^2\delta/\gamma$, where Δv is the relative gas velocity.

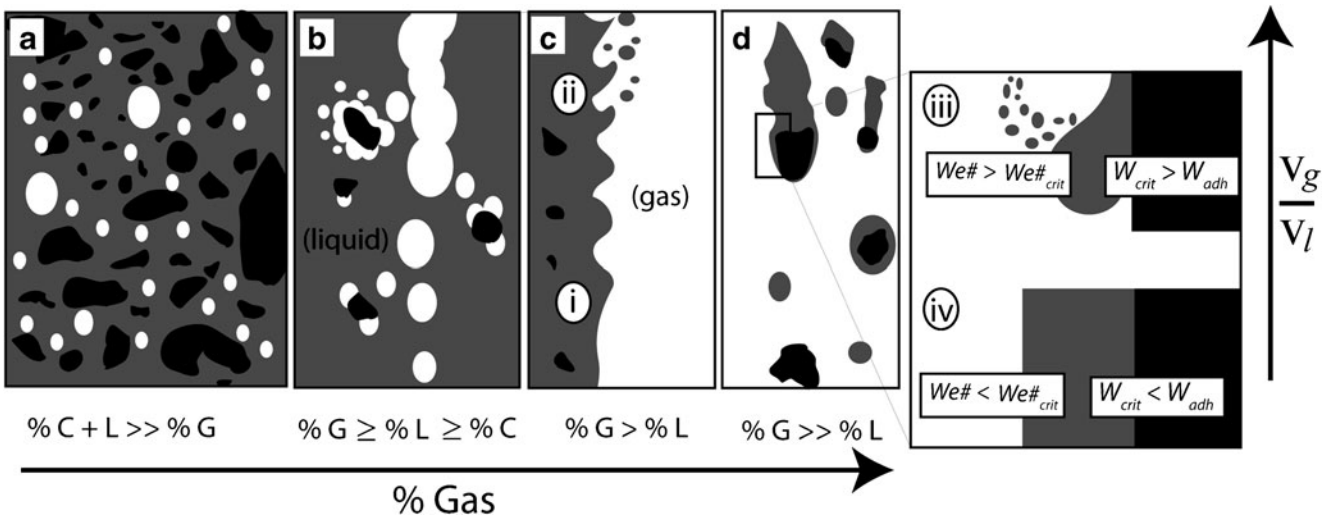

Fig. 8 Relationships in 3-phase (solid, liquid, gas) flow driven by progressive volumetric increase in gas content (*left* to *right*) and changing velocity ratios (v_g/v_l), and consequences for disruption of kimberlite: **a** relatively low gas content and high solids + melt content lead to fully coupled flow of solids (olivine), liquid (melt), and exsolved gases; **b** an increase in gas content (and corresponding dilution of solids and melt) leads to partial decoupling of solid–melt mixture from gas phase streaming through the low-viscosity melt. Nucleation of gas bubbles on olivine crystals may initiate first separation of melt from solids; **c** higher gas fractions promote greater decoupling and an increasing velocity contrast between liquid and gas, creating two kinds of fluid mechanical instabilities at interface: (i) Kelvin–Helmholz and (ii) Rayleigh–Taylor (see footnotes 2 and 3 in the text); **d** gas fractions >> liquid + solids lead to fully fluidized magma. The high velocity and large volume of the gas phase lead to 'stripping' of liquid from solids. The *enlarged box* shows gas–liquid–solid interfaces and critical relationships for Weber numbers (We, We_c; Eq. 7), work of dispersion, and work of adhesion (W_{crit}, W_{adh}; Eqs. 7, 9) required for (iii) 'stripping' of melt from olivine crystals, and (iv) relaxation of liquid on solid surfaces due to surface tension forming rounded pyroclasts

dependent on flow conditions (i.e. Re) and a shape factor (F) and is calculated from:

$$C_D = \frac{24}{\mathrm{Re}} F^{-0.32} + 2\sqrt{1.07 - F} \quad (4)$$

The appropriate Re is computed as:

$$\mathrm{Re} = \frac{U_T \cdot d \cdot \rho_g}{\eta_g}. \quad (5)$$

where d is particle diameter, ρ_g is gas density, U_T is settling velocity, and η_g is gas viscosity. The differential velocity (U_T) of spherical pyroclasts (F=1) within the gas flux is then calculated for the appropriate Re using the expression:

$$U_T = \sqrt{\frac{0.75 d(\rho_c - \rho_g) g}{C_D \rho_g}} \quad (6)$$

These equations are used iteratively to converge on a final differential velocity (cf. Freundt and Bursik 1998) which represents the velocity difference between a settling spherical pyroclast and an expanding host gas at the base of the pipe-shaped conduit. For $\eta_g = 4\times10^{-4}$ Pa s (i.e. H_2O/CO_2 gas, ~1,000 m below surface at 1,000°C), d of 0.01 m, ρ_c= 3,000 kg m^{-3}, ρ_g=55 kg m^{-3}, and C_D=0.53, the U_T is 2.72 ms^{-1}. If gas exit velocities similar to estimates for other low-viscosity magmas (Wilson 1980; e.g. 106–476 ms^{-1}; Walker et al. 1984) can be assumed for kimberlite eruptions, it would imply a minimum net upward particle velocity of hundreds of metres per second, with a velocity differential of only a few metres per second for particle sizes similar to those observed in kimberlite deposits. The erupting flux of gas + melt + solid will also feel the drag of conduit walls which is likely to produce strong velocity gradients across the conduit; these gradients may allow for localized, transient domains where velocity differentials between the gas phase and melt + solids fraction are even higher.

Velocity differentials are a key influence in conversion of bulk liquid into a spray or mist (i.e. collection of drops), known as 'atomization' (Villermaux 2007). Atomization is triggered when the relative magnitude between inertial (i.e. stagnation pressure) and curvature (i.e. capillary restoring pressure) forces for droplets of liquid in a gas suspension exceeds a critical value. This critical ratio can be expressed as a dimensionless critical Weber number (We_c):

$$We_c = (\rho_g(\Delta v)^2(d_0))/\gamma \quad (7)$$

where p_g is gas density, Δv is the velocity differential between liquid and gas, d_0 is the initial liquid droplet diameter, and γ is surface tension (N m^{-1}). One indication of high velocity contrasts (Δv) is the size distribution of the droplets created by atomization, as the size of droplets sprayed off from a liquid surface decreases with the velocity contrast (Faeth et al. 1995; Wu and Faeth 1995),

and scales as a function of energy input (Hinze 1959). If velocity contrasts are great enough between large clots, blebs, or droplets of kimberlite melt and ambient gas, the pieces of magma could efficiently disaggregate into much smaller droplets (Figs. 6 and 8d).

Olivine crystal content and melt separation

The olivine crystal content in kimberlite may also influence the disruption of the magma. For example, interfacial energies which cause kimberlite melt to preferentially wet the outer surfaces of olivine crystals clearly would also operate to inhibit separation of melt from crystals during eruption. The total surface area of a population of particles is a function of the abundance and size distribution of the particles. Thus, the abundance (i.e. modal per cent) and size distribution of olivine content within an erupting kimberlite magma may ultimately control the crystal-to-kimberlite ratios within juvenile pyroclasts, as well as the sizes of juvenile pyroclast produced.

To assess the influence of crystal content (i.e. modal per cent, surface area) on the ability of melt to separate from olivine crystals, we compare (a) olivine content (modal per cent) with sizes of JPs (melt-stripping of olivine during explosive eruption) and (b) estimated surface area of olivine crystals within JPs with estimated volumes of JPs. Olivine content (modal per cent) is plotted against size for all JPs from Fig. 6 in Fig. 10a and is subdivided according to textural relationships between olivine crystals and attached or enclosing kimberlite groundmass (Moss et al. 2009). These data indicate a general increase in olivine content with size for JPs with multiple olivine crystals (M, dashed lines; Fig. 9a). The surface areas of equivalent-radii spheres are calculated from the 2D intersections of olivine crystals within JPs and for JP outlines to find the ratio of estimated surface area of olivine within each juvenile pyroclast (SA_{ol}) to the estimated volume of kimberlite groundmass in each juvenile pyroclast (V_m) within the PK dataset. The estimated SA_{ol}: V_m ratio is plotted against the estimated size (V_{jp}) of the juvenile pyroclast in Fig. 9b. The SA_{ol} increases with the size of JP, but there is an overall decrease in the SA_{ol}:V_m ratio with an increase in the size of JP. Thus, olivine content (modal per cent) and surface area (SA_{ol}) both show positive correlations with the size of JP. The overall decrease in SA_{ol}:V_m with increasing size of JP may be due to more boundary-layer effects between neighbouring olivine crystals and the decreasing influence of surface tension on retaining the liquid volume of a droplet with an increase in the size (i.e. surface area) of the droplet of magma.

For a gas phase to separate a melt from a solid surface, a dispersive pressure (kg s^{-2} m^{-1}) applied to the outer surface of the melt-wetted solid must overcome the work of adhesion (W_{adh}) which couples the melt to the solid (Bangham and Razouk 1937), defined by the Young–Dupree equation:

$$W_{adh} = \gamma(1 + \cos\theta) \quad (8)$$

where γ is the liquid surface tension and θ is the contact angle between solid and liquid. W_{adh} has the same units as surface tension (kg s^{-2}) and is equivalent to work per unit area (Nm m^{-2}). Thus, the total work required to separate liquid from a solid surface increases proportionally with increasing total surface area (e.g. crystal surfaces).

Thin, complete selvages of kimberlite on olivine crystals (radius ~0.1 mm) and low contact angles (approx. 10–30°) between olivine crystals and partial

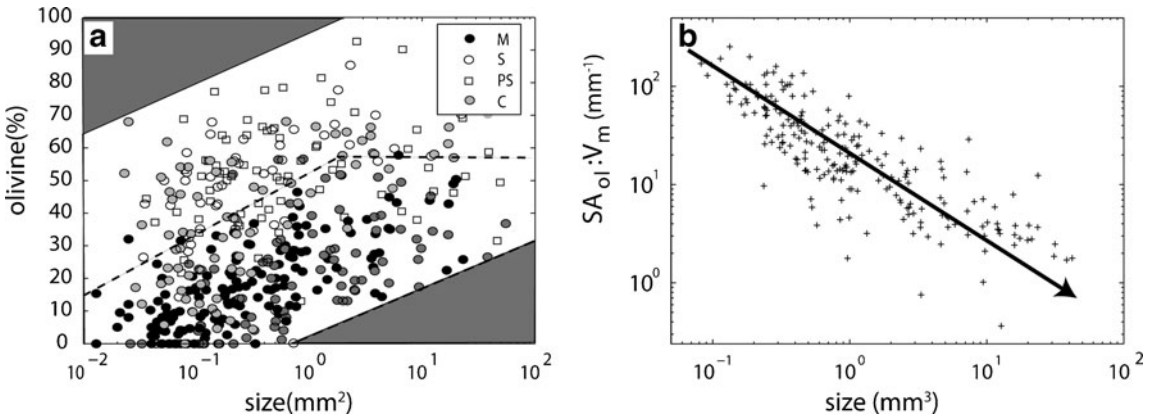

Fig. 9 Textural and geometric properties of juvenile pyroclasts of kimberlite: **a** olivine content (per cent) vs. size (square millimetres) of pyroclast for: pyroclasts containing multiple olivine crystals (*M*), olivine crystals with selvages of kimberlite groundmass (*S*), olivine grains with partial selvage (*PS*), and cored pyroclasts (*C*); **b** computed 3D surface area (square millimetres) of all olivine grains within individual pyroclasts (SA_{ol}) ratioed to the model 3D volume of kimberlite groundmass (cubic millimetres) within enclosing pyroclast (V_m) plotted against size of pyroclast (cubic millimetres). Note the decrease in SA_{ol}/V_m ratio with increasing size of pyroclast (*arrow*)

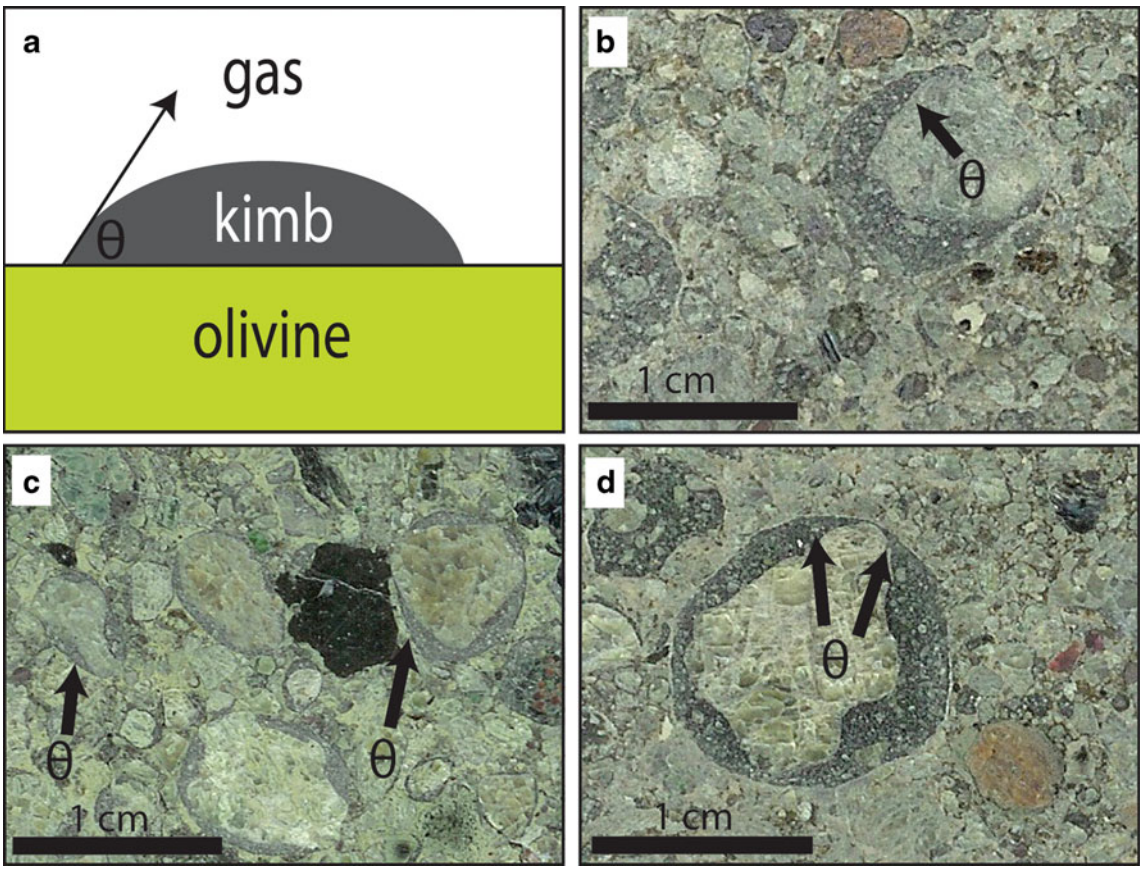

Fig. 10 Wetting angles between olivine crystals and kimberlite for pyroclasts in PK: **a** schematic showing the wetting angle (θ) between kimberlite melt (*kimb*) and crystal in a gas medium; **b**–**d** examples of large (~0.01 m) juvenile pyroclasts comprising a large olivine crystal 'core', incompletely coated by kimberlite. Note low contact angles (θ<30°) between kimberlite and olivine crystals

selvages of kimberlite are observed in many juvenile pyroclasts in PK (Fig. 10b–d). Such low contact angles indicate an attraction between the olivine and adjoining liquid melt (W_{adh}) that exceeds the cohesive strength of the melt (i.e. work of cohesion). As the gas fraction rises, the melt preferentially wets the olivine. The W_{adh} for a variety of liquids having viscosities near that of kimberlite melt (e.g. 0.1–10 Pa s; Sparks et al. 2006) is modelled for different contact angles (θ=0–180°) in Fig. 11a. Observations of contact angles between kimberlite and olivine crystals on the outside margin of juvenile pyroclasts suggest a likely range for W_{adh} required to separate melt from olivine crystals (Fig. 11a, shaded region; W_{adh}=0.2–0.8 kg s^{-2}).

The sizes, morphologies, and types of pyroclasts produced by an explosive eruption of low-viscosity kimberlite magma are influenced by: (a) the ratio of inertial to curvature forces (We_c), (b) the energy per unit area of melt adhering to crystals (W_{adh}), and (c) stagnation pressure $\left(\rho_g \cdot \left(\Delta v\right)^2\right)$ of fluxing volcanic gases. We can model the critical conditions needed for both 'atomization' of the melt and 'stripping' crystals of melt by considering when W_{adh} is exceeded by dispersive forces encapsulated by a 'critical' work term (W_c):

$$W_c > W_{adh} > \gamma(1+\cos\theta) \tag{9}$$

We can replace the term for surface tension by a rearranged form of Eq. 7 to obtain an expression that contains eruption (velocity contrast) and pyroclast (size) properties:

$$W_c > \left[\frac{(1+\cos\theta)\cdot\rho_g\cdot d_o}{We_c}\right](\Delta v)^2 \tag{10}$$

We have modelled these critical conditions required to 'atomize' kimberlite melt and 'strip' melt from crystal surfaces. The gas phase is assumed to be equal parts CO_2 and H_2O and has a density of 55 kg m^{-3} dictated by the pressure conditions (~15 MPa) in an open conduit 1,000 m below surface, lifting a partially expanded flux (50% gas) of kimberlite magma (Fig. 11b). The model considers pyroclasts with d_0 of 0.01, 0.05, and 0.001 m and with selvage–solid interfacial angles of θ of 15°. The critical Weber number (i.e. We_c) for atomization of silicate and

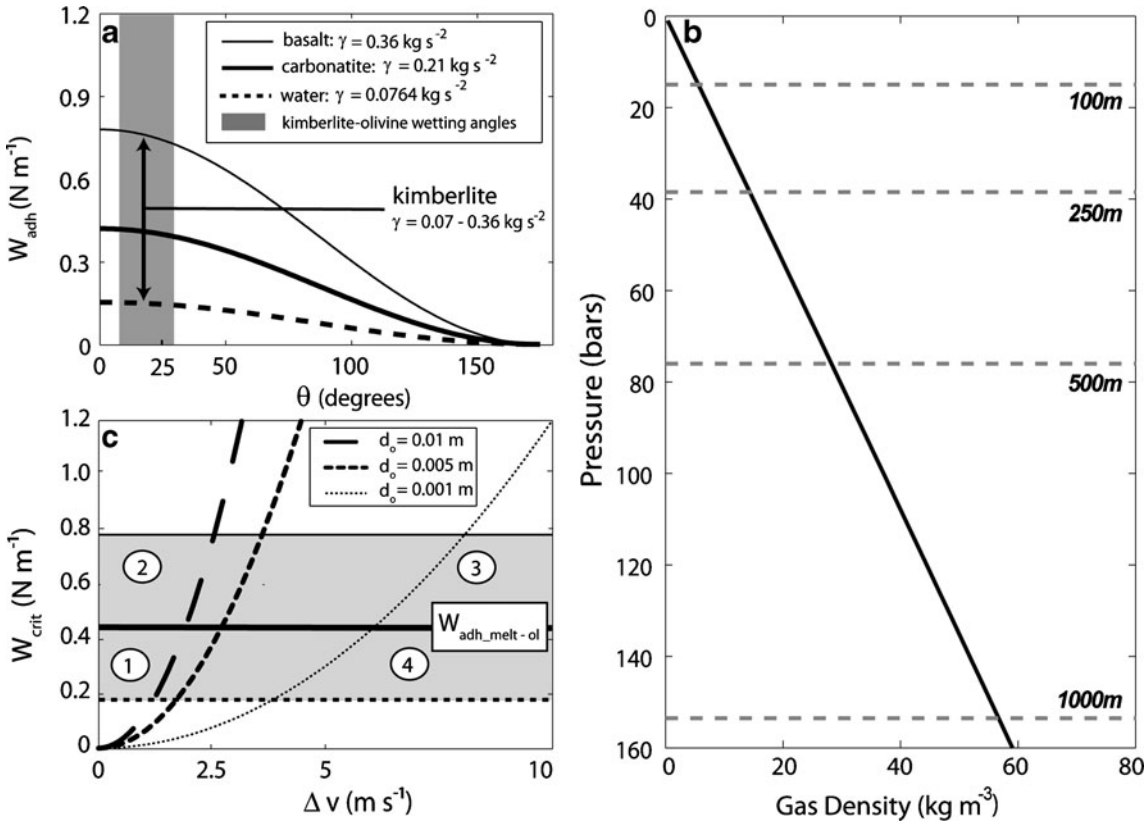

Fig. 11 Model conditions for gas-stripping of kimberlite melt from olivine crystals (see text for full explanation): **a** work of adhesion (W_{adh}; Eq. 8) vs. wetting angle between liquid and a solid surface (θ) for basalt melt (*thin solid line*; γ=0.36 kg s^{-2} from Walker and Mullins (1981), carbonatite melt (thick *solid line*; γ=0.21 kg s^{-2} from Wolff (1994), and water (*coarse dashed line*; surface tension γ= 0.0764 kg s^{-2}). The *shaded region* indicates range of observed contact angles between kimberlite selvages and exterior surface of olivine crystals; **b** computed density of exsolved fluid phase as a function of pressures corresponding to depths of 0–1,000 m; calculations assume a 1:1 molar ratio of H_2O/CO_2 pressurized by an overlying expanding flux of magma having on average 50% gas fraction and using a melt + solid density of 3,000 kg m^{-3}. **c** Four fields (*1–4*) marking transitions in melt–crystal relationships defined by intersection of W_{adh} at melt–olivine interfaces and the curve for W_c as a function of Δv for melt droplets 0.01, 0.005, and 0.001 m in diameter and assuming We_c similar to that of water. Specific values of $W_{adh\ melt\text{-}ol}$ for assumed basalt, carbonatite, or water-similarity with kimberlite melt are shown as *horizontal lines* (*thin*, *thick*, and *dashed* lines, respectively). The fields for interactions between kimberlite melt and olivine crystals are: (1) no 'atomization' or stripping of melt from crystals; (2) no 'atomization', but melt is stripped from crystals; (3) both 'atomization' and stripping of melt from crystals; (4) 'atomization' of liquid but no stripping of liquid from crystals

carbonate melts is unknown, and thus, given the low viscosity of kimberlite, we have used a value similar to that of water (~10; Wierzba 1990).

Equation 10 is used to map the critical relationships between velocity contrasts and 'critical' work (W_c) required to achieve four end-member relationships between kimberlite melt and olivine crystals (Fig. 11c): (1) kimberlite melt is neither separated from olivine crystals (i.e. $W_c < W_{adh}$) nor 'sprayed' or 'atomized' ($We < We_c$); (2) kimberlite melt is separated from olivine crystals (i.e. $W_c > W_{adh}$), but is not 'sprayed' or 'atomized' by the flux of surrounding gas ($We < We_c$); (3) both melt separation (i.e. $W > W_{adh}$) and 'atomization' ($We > We_c$); (4) kimberlite melt remains attached to olivine crystals (i.e. $W_c < W_{adh}$), but droplets are 'sprayed' or 'atomized' by the flux of surrounding gas ($We > We_c$).

Implications for the volcanic eruption of kimberlite

Interpretation

In this section, we discuss the processes implied by observations made above. First, olivine crystals are shown to be modified due to explosive eruption. These changes in sizes and shapes of olivine grains are efficiently tracked by D values of olivine crystal size distributions. Changes in these model D values are most likely the result of pressure drops and thermal shocks experienced by the ascending magma. We interpret the most likely cause for crystal breakage to be the pressure differential during eruption: rapid pressure changes induced by turbulent behaviour within an ascending and/or erupting kimberlite magma could facilitate breakup or fragmentation of olivine crystals

along internal, pre-conditioned areas of weakness. Thus, we suggest *D* values of olivine CSDs are modified in proportion to the change in pressure experienced by the magma and serve as a gauge of the violence of kimberlite eruption.

Second, it has been shown that pyroclastic deposits contain both kimberlite-free olivine and juvenile pyroclasts comprising olivine crystals enclosed by kimberlite. Gas contents, exit velocities, or velocity contrasts in an erupting kimberlite magma can be reflected in pyroclastic products of kimberlite eruptions in two ways: (1) the relative ratios of juvenile pyroclasts of kimberlite (JPs) to free olivine crystals observed in a deposit (FO) and (2) the size distribution of JPs (i.e. droplets of kimberlite enclosing olivine) produced during eruption. Therefore, olivine crystal and kimberlite textures in pyroclasts suggesting high velocity contrasts (e.g. 'stripped' olivine crystals) imply greater gas content in the erupting kimberlite magma. Moreover, differences in the degree of melt-stripping (i.e. FO/JP ratios) among or within pyroclastic deposits likely reflect differences in gas content in the magma from which the pyroclasts derive. In addition, the higher olivine content and corresponding surface area observed in larger JPs suggest that primary breakup of kimberlite magma and secondary breakup of un-solidified pyroclasts by melt 'stripping' are attenuated by high olivine contents and may lead to a biassed preservation of: (a) pyroclasts with higher olivine contents (and surface areas) in pyroclastic deposits relative to the starting magma and (b) larger pyroclasts with higher olivine contents than smaller pyroclasts. The gas content of erupting kimberlite magma is also known to correlate with eruption column height in other low-viscosity magmas (e.g. Parfitt et al. 1995), suggesting the FO/JP ratio may also be a proxy for the power of the eruption. Thus, we suggest that the volumetric properties of gas, melt, and solids determine how readily melt can separate from crystals in low-viscosity kimberlite magma, and these phase proportions can be approximated by the FO/JP ratios in deposits.

New eruption index

The observation of diverse pyroclast assemblages in pyroclastic deposits worldwide implies that eruption dynamics for kimberlite vary from volcano to volcano (Table 1). Though efforts have been made to create a single index (e.g. Volcano Explosivity Index; Newhall and Self 1982) which can effectively account for a variety of conventional metrics (magnitude, intensity, peak eruption height, energy release, power output, destructive potential), such indices are incapable of describing the behaviour of all volcanic eruptions (Sigurdsson 2000).

Many of these indices are based on observations and measurements of actual eruptions (e.g. peak eruption plume height); others have been created to correlate the eruption with the resulting pyroclastic deposit (e.g. magnitude= $\log_{10}$(erupted mass, kg)−7). Walker (1973) suggested using grain size properties and areal extent of pyroclastic deposits for comparative purposes and to deduce style and energy from pyroclastic deposits (Walker 1973; Cas and Wright 1987). These parameters were designed to reflect the rate of energy release and the manner in which it is released during volcanic eruption (Walker 1973).

Kimberlite volcanoes rarely preserve extra-crater deposits that would support this type of analysis. For example, poor exposure of extra-crater deposits and post-emplacement alteration mean it is only possible to constrain minimum estimates of mass involved in eruptions from kimberlite pipes (Porritt et al. 2008). In addition, no one has ever observed a kimberlite eruption, requiring models or inferences of the peak eruption heights and exit velocities based on physical properties of kimberlite magmas (Russell et al. 2006; Sparks et al. 2006). Debates concerning the depositional styles (e.g. fall, surge, flow, fluidized fountain) responsible for pyroclastic deposits found within kimberlite pipes (Walters et al. 2006; Gernon et al. 2008; Porritt et al. 2008) are hampered because Walker's *D* and *F* indices (Walker 1973) are designed for extra-crater fallout deposits (rather than within vent/conduit deposits).

On this basis, we present a new fragmentation index for kimberlite eruptions that can be applied to any pyroclastic kimberlite deposit. Caution must be taken to ensure the deposit is sufficiently fresh such that representative measurements can be made for either all of the olivine population or all of the juvenile pyroclasts. The index is a metric for the relative fragmentation intensity attending kimberlite eruptions (Fig. 12) and is based on data collected from coherent and pyroclastic rocks, models of dynamical fluid behaviour, and is in the spirit of the original *F–D* diagram of Walker (1973).

Slopes from power–law approximations of olivine crystal populations (Moss et al. 2010) or '*D*' values are used to characterize the extent to which olivine crystals have broken during eruption ('*D*' values; Fig. 12). *D* values are useful because they are scale-independent (i.e. dimensionless) and require significant changes in the overall properties of olivine crystal populations to change their values (Kaminski and Jaupart 1998; Walters et al. 2006). If changes in *D* values correlate with the magnitude of pressure changes, the '*D*' parameter is then analogous to Walker's '*F*' (Walker 1973) as a proxy for violence of eruption, and may be highly affected by environmental influences. For example, external groundwater, vent clogging (after Walker 1973), or overpressures built up by cap-

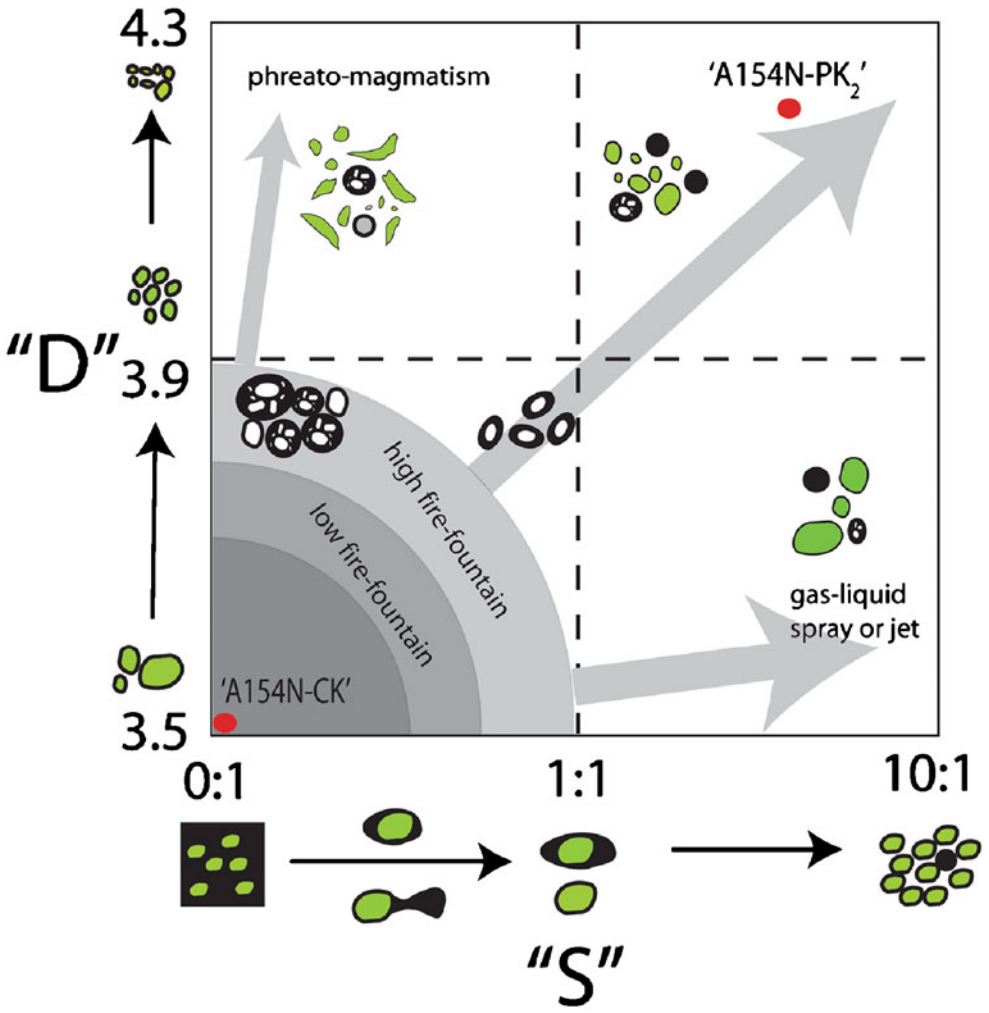

Fig. 12 Fragmentation index proposed for eruption of kimberlite magmas (KFI) based on properties of pyroclastic deposits of kimberlite, on the basis of: (i) *D* values for linear fits to olivine crystal size distributions (cf. Fig. 4) and (ii) the separation ratio, '*S*', which is taken as the (volumetric) ratio of 'free' olivine crystals (FO) to the volume fraction of kimberlite pyroclasts that enclose olivine crystals (JP). CSD slopes are dimensionless, are expected to correlate with eruption overpressures, and are analogous to Walker's fragmentation (i.e. '*F*') parameter (Walker 1973). The separation ratio, '*S*', is also dimensionless, reflects the intrinsic power of the eruption, and is controlled by the gas fraction of the eruption flux and the velocity differential between gas and magma (melt + solids). Two kimberlite deposits from the present study are plotted as *red dots*: intrusive coherent kimberlite dykes (*A154N-CK*) and pyroclastic kimberlite (*A154N-PK*). Hypothetical eruption styles (e.g. *phreato-magmatism*, *high fire-fountain*) are attributed to variable '*S*' vs. '*D*' textural relationships. Further data collection from kimberlite deposits is required to establish these relationships

rocks (e.g. Field and Scott Smith 1999) can lead to more violent explosions and, therefore, a higher *D* value.

The FO/JP ratio is used to characterize the degree to which melt has separated from crystals during eruption ('*S*' values; Fig. 12). This ratio is useful because it can be measured at many scales of observation and because it does not require a dataset which includes all of the eruptive products of kimberlite eruptions. Thus, deposits contained within the vent of a kimberlite volcano (i.e. many intra-pipe deposits) can be examined, and it is not necessary to know the full lateral or extra-vent extent of ash (crystalline or quenched kimberlite w/o olivine crystals) deposition in order to determine a reasonable estimate FO/JP ratio. Many of the possible causes for separation discussed above depend upon the gas content and velocity. Eruption column height and transport distance are also directly related to gas content and are a proxy for the 'power' of an eruption. The '*S*' parameter strongly correlates to the power of the gas blast, is the most affected by relative proportions of phases intrinsic in the magma, and is thus analogous to Walker's '*D*' (Walker 1973). For example, increasing magma viscosity, exsolved gas content, or the depth at which gas bubbles begin to form can lead to explosions with a higher '*S*' value.

Characterizing kimberlite eruptions using this fragmentation index has several applications. First, the index can assist in identifying the volcanic facies (i.e. pyroclastic vs. effusive, welding, etc.) of kimberlite. Secondly, the index may be used to assess the relative intensity (i.e. kilogrammes per second, exit velocity and volatile content) of kimberlite eruptions. Thirdly, the index may act as a tool for evaluating potential diamond grade enhancement or diminishment for a pyroclastic deposit of kimberlite.

Caveat emptor

An important assumption before using this index is that the deposits in kimberlite pipes are representative of the entire range of pyroclasts produced within a kimberlite eruption. However, elutriation and loss of ash or fines may lead to a bias in preservation (Nowicki et al. 2008; Porritt et al. 2008). The result would be deposits with higher olivine contents and lower kimberlite contents than was actually produced by the eruption. Moreover, alteration of kimberlite ash and the smallest fraction of olivine crystals and crystal fragments in the matrix of pyroclastic rocks may mask its presence in the original deposit. This will also cause an overestimation of olivine content and underestimation of the original melt fraction. However, a key point to remember is that we are only concerned with the degree to which melt has separated from olivine crystals (FO/JP). This is a relative relationship and can be adequately captured if one is confident they have made representative observations of either all of the olivine crystals or all of the JPs.

Acknowledgements This research was funded by an NSERC Collaborative Research and Development Grant (22R42415) held by J.K. Russell and sponsored by RioTinto Diavik Diamond Mine, Inc. (DDMI), entitled Kimberlite Eruption Dynamics: Implications for Diamond Distribution in the Diavik Kimberlite. We gratefully acknowledge critical reviews by RSJ Sparks, Richie Brown, Alison Rust, and James White, as well as constructive conversations with Barbara Scott Smith, Lucy Porritt, and Bram van Straaten.

References

Arndt NT, Boullier AM, Clement JP, Dubois M, Schissel D (2006) What olivine, the neglected mineral, tells us about kimberlite petrogenesis. eEarth 1:15–21

Bangham DH, Razouk RI (1937) Adsorption and wettability of solid surfaces. Trans Faraday Soc 33:1459–1463

Basson IJ, Viola G (2004) Passive kimberlite intrusion into actively dilating dyke-fracture arrays: evidence from fibrous calcite veins and extensional fracture cleavage. Lithos 76(1–4):283–297

Best MG, Christiansen EH (1997) Origin of broken phenocrysts in ash-flow tuffs. Geol Soc Am Bull 109(1):63–73

Bindeman IN (2005) Fragmentation phenomena in populations of magmatic crystals. Am Mineral 90:1801–1815

Blake S, Wilson CJN, Smith IEM, Walker GPL (1992) Petrology and dynamics of the Waimihia mixed magma eruption, Taupo Volcano, New Zealand. J Geol Soc 149(2):193–207. doi:10.1144/gsjgs.149.2.0193

Blander M, Katz JL (1975) Bubble nucleation in liquids. AICHE J 21 (5):833–848

Bonnet E, Bour O, Odling NE, Davy P, Main I, Cowie P, Berkowitz B (2001) Scaling of fracture systems in geological media. Rev Geophys 39(3):347–383

Boyer L, Hood CT, McCandless TE, Skelton D, Tosdal RM (2004) Volcanology of the Buffalo Hills Kimberlites, Alberta, Canada: some preliminary observations. 8th International Kimberlite Conference Long Abstract

Brett RC, Russell JK, Moss S (2009) Origin of olivine in kimberlite: phenocryst or impostor? Lithos 112(Supplement 1):201–212

Brown RJ, Gernon T, Stiefenhofer J, Field M (2008) Geological constraints on the eruption of the Jwaneng Centre kimberlite pipe, Botswana. J Volcanol Geotherm Res 174(1–3):195–208

Bursik M (1998) Tephra dispersal. In: Gilbert JS, Sparks RSJ (eds) The physics of explosive volcanic eruptions, vol 145. Geol Soc Spec Pub, pp 115–144

Cas RAF, Wright JV (1987) Volcanic successions, modern and ancient. Chapman & Hall, London

Cas R, Porrit L, Hayman P, Pittari A (2008) Pyroclast formation processes during explosive kimberlite eruptions. 9th International Kimberlite Conference, extended abstract no. 9IKC-A-00030

Clauset A, Shalizi CR, Newman MEJ (2007) Power-law distributions in empirical data. arXiv 0706_1062v1:1–26

Clement CR (1982) A comparative geological study of some major kimberlite pipes in the Northern Cape and Orange Free State. University of Cape Town, Cape Town, South Africa

Downes PJ, Ferguson D, Griffin BJ (2007) Volcanology of the Aries micaceous kimberlite, central Kimberley Basin, Western Australia. J Volcanol Geotherm Res 159(1–3):85–107

Dunbar NW, McIntosh WC, Esser RP (2008) Physical setting and tephrachronology of the summit caldera ice record at Mount Moulton, West Antarctica. Geol Soc Am Bull 120(7–8):796–812

Faeth G, Hsiang L-P, Wu P-K (1995) Structure and breakup properties of sprays. Int J Multiphase Flow 21:99–127

Field M, Scott-Smith BH (1999) Contrasting geology and near-surface emplacement of kimberlite pipes in southern Africa and Canada. In: VIIth International Kimberlite Conference, Cape Town, South Africa. Red Roof Designs, pp 214–237

Fisher RV (1963) Bubble-wall texture and its significance. J Sediment Res 33:224–227

Fitzgerald CE, Hetman CM, Lepine I, Skelton DS, McCandless TE (2009) The internal geology and emplacement history of the Renard 2 kimberlite, Superior Province, Quebec, Canada. Lithos 112(Supplement 1):513–528

Freundt A, Bursik MI (1998) Pyroclastic density currents. In: Gilbert JS, Sparks RSJ (eds) The physics of explosive volcanic eruptions, vol 145. Geol Soc London Special Pub, pp 145–182

Galloway M, Nowicki T, van Coller B, Mukodzani B, Siemens K, Hetman C, Webb K, Gurney J (2009) Constraining kimberlite geology through integration of geophysical, geological and geochemical methods: a case study of the Mothae kimberlite, northern Lesotho. Lithos 112(Supplement 1):130–141

Gernon TM, Gilbertson MA, Sparks RSJ, Field M (2008) Gas-fluidisation in an experimental tapered bed: insights into processes in diverging volcanic conduits. J Volcanol Geotherm Res 174(1–3):49–56

Gernon TM, Fontana G, Field M, Sparks RSJ, Brown RJ, Mac Niocaill C (2009) Pyroclastic flow deposits from a kimberlite eruption: The Orapa South Crater, Botswana. Lithos 112 (1):556–578

Giordano D, Russell JK, Dingwell DB (2008) Viscosity of magmatic liquids: a model. Earth Planet Sci Lett 271(1–4):123–134

Gonnermann HM, Manga M (2007) The fluid mechanics inside a volcano. Ann Rev Fluid Mech 39(1):321–356. doi:10.1146/annurev.fluid.39.050905.110207

Graham I, Burgess JL, Bryan D, Ravenscroft PJ, Thomas E, Doyle BJ, Hopkins R, Armstrong KA (1999) Exploration history and geology of the Diavik kimberlites, Lac de Gras, Northwest Territories, Canada. In: Gurney JJ, Gurney JL, Pascoe MD, Richardson SH (eds) Proceedings of the VIIth International Kimberlite Conference, Cape Town, South Africa. Red Roof Design, pp 262–279

Hammer JE, Coombs ML, Shamberger PJ, Kimura J-I (2006) Submarine sliver in North Kona: a window into the early magmatic and growth history of Hualalai Volcano, Hawaii. J Volcanol Geotherm Res 151(1–3):157–188

Harder M, Scott Smith BH, Hetman CM, Pell J (2009) The evolution of geological models for the DO-27 kimberlite, NWT, Canada: implications for evaluation. Lithos 112(Supplement 1):61–72

Harvey S, Kjarsgaard B, McClintock M, Shimell M, Fourie L, Du Plessis P, Read G (2009) Geology and evaluation strategy of the Star and Orion South kimberlites, Fort a la Corne, Canada. Lithos 112(1):47–60

Head JW, Wilson L (2008) Integrated model for kimberlite ascent and eruption. 9th International Kimberlite Conference Extended Abstracts: 1–3

Heiken G (1972) Morphology and petrography of volcanic ashes. Geol Soc Am Bull 83(7):1961–1988. doi:10.1130/0016-7606(1972)83[1961:mapova]2.0.co;2

Herd RA, Pinkerton H (1997) Bubble coalescence in basaltic lava: its impact on the evolution of bubble populations. J Volcanol Geotherm Res 75(1–2):137–157

Hetman CM, Scott Smith BH, Paul JL, Winter F (2004) Geology of the Gahcho Kue kimberlite pipes, NWT, Canada: root to diatreme magmatic transition zones. Lithos 76(1–4):51–74

Higgins MD (2000) Measurement of crystal size distributions. Am Mineral 85:1105–1116

Hinze JO (1959) Turbulence, an introduction to its mechanisms and theory. McGraw-Hill, New York

Inman DL (1952) Measures for describing the size distribution of sediments. J Sediment Petrol 22:125–145

Kamenetsky VS, Kamenetsky MB, Sobolev AV, Golovin AV, Demouchy S, Faure K, Sharygin VV, Kuzmin D (2007) Olivine in the Udachnaya-East Kimberlite (Yakutia, Russia): types, compositions and origins. J Petrol 00:1–17

Kamenetsky VS, Kamenetsky MB, Sobolev AV, Golovin AV, Demouchy S, Faure K, Sharygin VV, Kuzmin DV (2008) Olivine in the Udachnaya-East kimberlite (Yakutia, Russia): types, compositions and origins. J Petrol 49(4):823–839

Kaminski E, Jaupart C (1998) The size distribution of pyroclasts and the fragmentation sequence in explosive volcanic eruptions. J Geophys Res 103:29759–29779

Kjarsgaard B, Harvey S, McClintock M, Zonneveld JP, Du Plessis P, McNeil D, Heaman L (2009) Geology of the Orion South kimberlite, Fort a la Corne, Canada. Lithos 112(1):600–617

Kueppers U, Perugini D, Dingwell DB (2006) "Explosive energy" during volcanic eruptions from fractal analysis of pyroclasts. Earth Planet Sci Lett 248(3–4):800–807

Kurszlaukis S, Barnett WP (2003) Volcanological and structural aspects of the Venetia kimberlite cluster — a case study of South African kimberlite maar–diatreme volcanoes. S Afr J Geol 106:165–192

Kurszlaukis S, Mahotkin I, Rotman AY, Kolesnikov GV, Makovchuk IV (2006) Syn- and post-eruptive volcanic processes in the Yubileinaya kimberlite pipe, Yakutia. Kimberlite Emplacement Workshop, long abstract: 1–5

Leckie DA, Kjarsgaard BA, Bloch J, McIntyre D, McNeil D, Stasiuk L, Heaman L (1997) Emplacement and reworking of Cretaceous, diamond-bearing, crater-facies kimberlite of central Saskatchewan, Canada. Geol Soc Am Bull 109(8):1000–1020

Mahotkin I, Robey J, Kurszlaukis S, Valuev E, Pylaev N (2003) Pipe emplacement model of the Lomonosov diamond deposit, Archangelsk region, NW Russia. Eighth International Kimberlite Conference Long Abstract

Mainkar D, Lehmann B, Haggerty SE (2004) The crater-facies kimberlite system of Tokapal, Bastar District, Chhattisgarh, India. Lithos 76(1–4):201–217

Masun KM, Scott Smith BH (2008) The Pimenta Bueno kimberlite field, Rondônia, Brazil: tuffisitic kimberlite and transitional textures. J Volcanol Geotherm Res 174(1–3):81–89

Michol KA, Russell JK, Andrews GDM (2008) Welded block and ash flow deposits from Mount Meager, British Columbia, Canada. J Volcanol Geotherm Res 169(3–4):121–144

Mitchell RH (2009) Mineralogy of juvenile lapilli in Fort a la Corne pyroclastic kimberlites. Paper presented at the 2009 Joint Assembly AGU-GAC, Toronto, ON

Morgan DJ, Jerram DA (2006) On estimating crystal shape for crystal size distribution analysis. J Volcanol Geotherm Res 154(1–2):1–7

Moss S, Russell JK, Andrews GDM (2008) Progressive infilling of a kimberlite pipe at Diavik, Northwest Territories, Canada: insights from volcanic facies architecture, textures, and granulometry. J Volcanol Geotherm Res 174(1–3):103–116

Moss S, Russell JK, Brett RC, Andrews GDM (2009) Spatial and temporal evolution of kimberlite magma at A154N, Diavik, Northwest Territories, Canada. Lithos 112(Supplement 1):541–552

Moss S, Russell JK, Smith BHS, Brett RC (2010) Olivine crystal size distributions in kimberlite. Am Mineral 95(4):527–536. doi:10.2138/am.2010.3277

Naidoo P, Stiefenhofer J, Field M, Dobbe R (2004) Recent advances in the geology of Koffiefontein Mine, Free State Province, South Africa. Lithos 76(1–4):161–182

Newhall CG, Self S (1982) The Volcano Explosivity Index (VEI): an estimate of explosive magnitude for historical volcanism. J Geophys Res 87(C2):1231–1238

Nowicki T, Crawford B, Dyck D, Carlson J, McElroy R, Oshust P, Helmstaedt H (2004) The geology of kimberlite pipes of the Ekati property, Northwest Territories, Canada. Lithos 76(1-4):1–27

Nowicki T, Porritt L, Crawford B, Kjarsgaard B (2008) Geochemical trends in kimberlites of the Ekati property, Northwest Territories, Canada: insights on volcanic and resedimentation processes. J Volcanol Geotherm Res 174(1–3):117–127

Parfitt EA (2004) A discussion of the mechanisms of explosive basaltic eruptions. J Volcanol Geotherm Res 134(1–2):77–107

Parfitt EA, Wilson L, Neal CA (1995) Factors influencing the height of Hawaiian lava fountains: implications for the use of fountain height as an indicator of gas content. Bull Volcanol 57:440–450

Pittari A, Cas RAF, Lefebvre N, Robey J, Kurszlaukis S, Webb K (2008) Eruption processes and facies architecture of the Orion Central kimberlite volcanic complex, Fort à la Corne, Saskatchewan; kimberlite mass flow deposits in a sedimentary basin. J Volcanol Geotherm Res 174(1–3):152–170

Porritt LA, Cas RAF (2009) Reconstruction of a kimberlite eruption, using an integrated volcanological, geochemical and numerical approach: a case study of the Fox Kimberlite, NWT, Canada. J Volcanol Geotherm Res 179(3–4):241–264

Porritt LA, Russell JK (2011) Kimberlite ash: Fact or fiction. Physics and Chemistry of the Earth, Parts A/B/C. doi:10.1016/j.pce.2011.03.002

Porritt LA, Cas RAF, Crawford BB (2008) In-vent column collapse as an alternative model for massive volcaniclastic kimberlite emplacement: an example from the Fox kimberlite, Ekati Diamond Mine, NWT, Canada. J Volcanol Geotherm Res 174(1–3):90–102

Price S, Russell JK, Kopylova M (2000) Primitive magma from the Jericho pipe, N.W.T., Canada: constraints on primary melt chemistry. J Petrol 41(6):789–808

Russell JK, Giordano D, Kopylova M, Moss S (2006) Transport properties of kimberlite melt. In: Long Abstract, Kimberlite Emplacement Workshop, Saskatoon, Canada

Schmincke HU (2004) Volcanism, 2nd edn. Springer, Berlin

Schumacher R, Schmincke H-U (1991) Internal structure and occurrence of accretionary lapilli — a case study at Laacher See Volcano. Bull Volcanol 53(8):612–634

Scott Smith BH (1995) Geology of the Sturgeon Lake 02 kimberlite block, Saskatchewan. Exploration and Mining Geology CIM 4: 141–151

Scott Smith BH (2008a) Canadian kimberlites: geological characteristics relevant to emplacement. J Volcanol Geotherm Res 174(1–3):9–19

Scott Smith BH (2008b) Introduction to kimberlites. Short course notes: kimberlites-geological principles relevant to evaluation, resource classification and mining. In: mineral exploration roundup 08, Vancouver, p 21

Scott Smith BH, Smith SCS (2009) The economic implications of kimberlite emplacement. Lithos 112(Supplement 1):10–22

Sigurdsson H (ed) (2000) Encyclopedia of volcanoes. Academic, San Diego

Sparks RSJ, Baker L, Brown RJ, Field M, Schumacher J, Stripp G, Walters A (2006) Dynamical constraints on kimberlite volcanism. J Volcanol Geotherm Res 155(1–2):18–48

Stiefenhofer J, Farrow DJ (2004) Geology of the Mwadui kimberlite, Shinyanga district, Tanzania. Lithos 76(1–4):139–160

Trickett SK, Jones AP, Field M (2006) Mapping lithofacies within the D/K1 kimberlite pipe, Letlhakane, Botswana: a multi-disciplinary approach. Kimberlite Emplacement Workshop, long abstract: 1–5

van Straaten BI, Kopylova MG, Russell JK, Webb KJ, Scott Smith BH (2008) Discrimination of diamond resource and non-resource domains in the Victor North pyroclastic kimberlite, Canada. J Volcanol Geotherm Res 174(1–3):128–138

Vergniolle S, Jaupart C (1986) Separated two-phase flow and basaltic eruptions. J Geophys Res 91(B12):12842–12860

Villermaux E (1998) On the role of viscosity in shear instabilities. Phy Fluids 10:368–373

Villermaux E (2007) Fragmentation. Ann Rev Fluid Mech 39:419–446

Walker GPL (1973) Explosive volcanic eruptions–a new classification scheme. Geol Rudsch 62:431–446

Walker D, Mullins O (1981) Surface tension of natural silicate melts from 1,200°–1,500°C and implications for melt structure. Contrib Mineral Petrol 76(4):455–462

Walker GPL, Self S, Wilson L (1984) Tarawera 1886, New Zealand–a basaltic plinian fissure eruption. J Volcanol Geotherm Res 21(1–2):61–78

Walters PJC, Brown RJ, Field M, Gernon T, Stripp G, Sparks RSJ (2006) The role of fluidisation in the formation of volcaniclastic kimberlite: grain size observations and experimental investigation. J Volcanol Geotherm Res 155(1–2):119–137

Webb KJ (2006) Juvenile clasts in kimberlites: standardizing comprehensive description towards unravelling emplacement models. In: Kimberlite Emplacement Workshop, Saskatoon, Saskatchewan

Webb KJ, Scott Smith BH, Paul JL, Hetman CM (2004) Geology of the Victor Kimberlite, Attawapiskat, Northern Ontario, Canada: cross-cutting and nested craters. Lithos 76(1–4):29–50

Wierzba A (1990) Deformation and breakup of liquid drops in a gas stream at nearly critical Weber numbers. Exp Fluids 9 (1):59–64

Wilson L (1980) Relationships between pressure, volatile content and ejecta velocity in three types of volcanic explosion. J Volcanol Geotherm Res 8(2–4):297–313

Wilson L, Parfitt EA (2008) Fundamentals of physical volcanology. Blackwell, Oxford

Wolff JA (1994) Physical properties of carbonatite magmas inferred from molten salt data, and application to extraction patterns from carbonatite-silicate magma chambers. Geol Mag 131:145–153

Wood BD, Scott Smith BH, de Gasparis S (1998) The ML kimberlitic pipes of northwest Alberta: exploration, geology and emplacement model. 7th International Kimberlite Conference Extended Abstracts, Cape Town, South Africa, 1998, J.J. Gurney, J.L. Gurney, M.D. Pascoe and S.H. Richardson (ed.); Red Roof Design cc, South Africa, pp. 960–962

Wu PK, Faeth GM (1995) Onset and end of drop formation along the surface of turbulent liquid jets in still gases. Phys Fluids 7 (11):2915–2917

Zonneveld JP, Kjarsgaard BA, Harvey SE, Heaman LM, McNeil DH, Marcia KY (2004) Sedimentologic and stratigraphic constraints on emplacement of the Star Kimberlite, east-central Saskatchewan. Lithos 76(1–4):115–138